acid. Recordings were obtained from dlBNST neurons visualized with infrared video microscopy (model IR-1000; Dage-MTI). Because dlBNST neurons have been categorized into three distinct types (Hammack et al., 2007), we first identified cell types by assessing the membrane potential responses to hyperpolarizing and depolarizing current injections. To monitor hyperpolarizing responses, we set the initial membrane potential at −60 mV and incremental currents (400 ms) ranging from 0 to −360 pA were injected. To monitor depolarizing and firing responses, we set the initial membrane potential at −80 mV, and incremental currents (400 ms) ranging from 0 to 160 pA were injected. Neurons that exhibited a depolarizing sag in response to hyperpolarizing current injection and a regular firing pattern in response to depolarizing current injection were classified as type I. Neurons that exhibited a depolarizing sag in response to hyperpolarizing current injection and burst firings in response to both the termination of the hyperpolarizing current injections and depolarizing current injections were classified as type II. Neurons that exhibited no depolarizing sag in response to hyperpolarizing current injection and a regular firing pattern in response to depolarizing current injection were classified as type III. Neurons were excluded from analyses if the amplitude of the action potential, which was determined as the difference between threshold and the peak, was <30 mV. Data were acquired with a Multiclamp 700B amplifier and the pClamp10 software (Molecular Devices).

Measurement of membrane potentials and input resistance. The initial membrane potentials were set to approximately –70 mV (–69.32 ± 0.23 mV, $n = 50$) by injecting negative or positive currents. To inhibit action potential-induced synaptic transmission, 500 nM TTX was added to superfused Ringer's solution. To monitor the changes in membrane potentials, a window with a 1 s duration was placed every 5 s, and the average membrane potential within the window was determined. To monitor changes in input resistance, input resistance was calculated by measuring the change in membrane potential evoked by a negative current (–80 pA, 200 ms) every 5 s. Then, the membrane potentials and input resistance during a 1 min period were calculated by averaging 12 of these values. After confirming stable membrane potentials and input resistance for >3 min, 1 μM CRF or 1 μM NPY was perfused through the recording chamber for 2 min except for the experiment shown in Figure 8, where NPY was perfused until the end of the experiment. In experiments assessing the effects of antagonists for CRF or NPY receptors on CRF- or NPY-induced change in membrane potentials, the antagonists were perfused for >10 min before bath application of CRF or NPY to the end of the experiments. Membrane potentials and input resistance were measured in the periods of 0–3 min before and 13–16 min after drug application. The latter period was chosen because the effects of CRF and NPY emerged gradually and became maximal in this period in most of the neurons tested. The effects of drugs were evaluated by comparing the average values observed during these two periods.

Analyses of steady-state membrane current–voltage relationships. Steady-state membrane current–voltage (*I–V*) relationships were examined in type II dlBNST neurons. Cells were voltage clamped at –70 mV in the presence of 1 μM TTX. To assess the *I–V* relationship, we used a voltage ramp protocol described in a previous study (Hara and Nakaya, 1997) with some modifications. Briefly, the membrane potential was first depolarized to 0 mV and then hyperpolarized to –120 mV at a rate of 0.1 mV/ms every 20 s. The current responses observed during the falling phase from –30 mV to –120 mV were used for *I–V* relationship analyses. Changes in net currents caused by a 2 min bath application of CRF or NPY were determined by subtracting the current responses to the voltage ramp in the periods of 0–3 min before drug application from those of 13–16 min after drug application. In some experiments, effects of NPY on *I–V* relationships were examined in the presence of ZD7288.

To measure holding currents, a window with a 1 s duration was placed every 20 s, and the average holding current within the window was determined. To monitor the changes in input resistance, input resistance was calculated by measuring the change in the holding current evoked by voltage steps (–5 mV, 30 ms) every 20 s. Holding currents and input resistance were measured in the periods of 0–3 min before and 13–16 min after drug application. The effects of drugs were evaluated by comparing the average values observed at these two periods.

Measurement of firing activity. To measure changes in firing activity, current-clamp recordings without current injection were carried out. To inhibit $GABA_A$ receptor-mediated and ionotropic glutamate receptor-mediated synaptic transmission, 10 μM SR95531 and 1 mM kynurenic

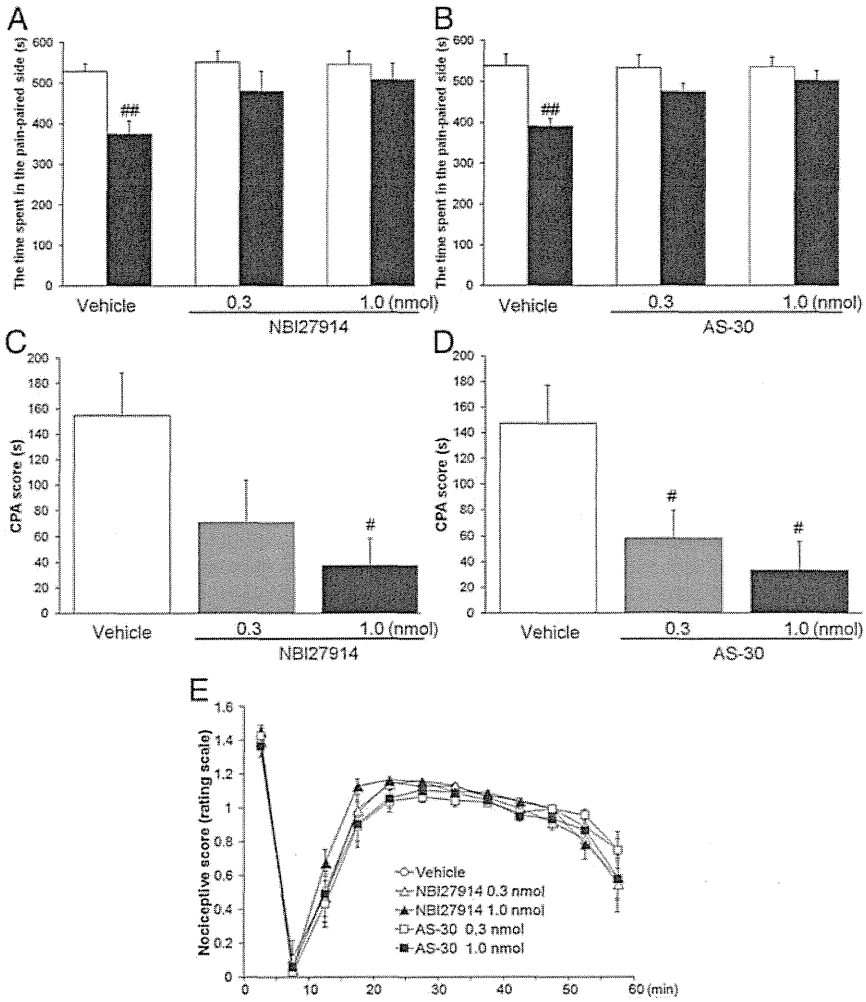

Figure 3. ***A–D***, Effects of intra-dlBNST injection of NBI27914 (***A***, ***C***, vehicle, $n = 7$; 0.3 nmol, $n = 8$; 1.0 nmol, $n = 7$) or AS-30 (***B***, ***D***, vehicle, $n = 6$; 0.3 nmol, $n = 6$; 1.0 nmol, $n = 7$) on formalin-induced CPA. Data are expressed as means ± SEM. The columns show the time spent in the pain-paired compartment in the preconditioning (white columns) and test (black columns) sessions (***A***, ***B***). $^{\#\#}p < 0.01$ compared with the preconditioning session (paired *t* test). The columns show the CPA scores (***C***, ***D***). $^{\#}p < 0.05$ compared with vehicle-injected rats (Newman–Keuls *post hoc* test). ***E***, Effects of intra-dlBNST injection of vehicle ($n = 11$), NBI27914 (0.3 nmol, $n = 6$; 1.0 nmol, $n = 7$), or AS-30 (0.3 nmol, $n = 6$; 1.0 nmol, $n = 6$) on formalin-induced nociceptive behaviors. Data are expressed as means ± SEM.

acid, respectively, were added to superfused Ringer's solution. To analyze firing activity, a window with 2.5 s duration was placed every 5 s, and the numbers of spikes in 36 windows were counted during 3 min. After counting basal firing activities, 1 μM CRF was perfused through the recording chamber for 2 min in the presence or absence of 1 μM NPY. NPY was perfused from 7.5 to 11 min before CRF application to the end of the experiments. Firing activities were measured during a period of 0–3 min before the application of peptides and 17–20 min after CRF application. The latter period was chosen because maximum firing activities were observed in this period in most of the neurons tested. The effects of drugs were evaluated by comparing the average values observed during these periods.

Statistical analyses. Data are expressed as means ± SEM. *In vivo* microdialysis data were assessed using one-way repeated-measures ANOVA followed by the Newman–Keuls *post hoc* test. Time spent in the pain- or drug-paired compartment during preconditioning and test sessions in the CPA test was analyzed using within-group paired *t* tests. CPA scores were analyzed using one-way ANOVA followed by the Newman–Keuls *post hoc* test or Student's *t* test for comparisons among more than two groups or between two groups, respectively. Two-way repeated-measures ANOVA was used for the data from measurements of nociceptive behaviors. Electrophysiological data were analyzed using the paired *t* test, Student's *t* test, or one-way repeated-measures ANOVA followed by the Newman–Keuls *post hoc* test. Statistical analyses were performed using IBM SPSS statistics v.20.0.0 or using GraphPad Prism v.6.00 (GraphPad Software); p values < 0.05 were considered to indicate statistically significant differences.

Results

Histology

After the *in vivo* microdialysis experiments and behavioral tests, histological analyses were performed. Data from rats with correct placements of the microdialysis probe (Fig. 1*A*) and of the bilateral microinjection cannulae (Fig. 1*B–E*) were used for the statistical analyses.

Pain-induced CRF release within the dlBNST

The averaged baseline concentration of CRF in the dialysates was 6.8 ± 0.5 pg/15 μl. Intraplantar injection of formalin produced a transient increase in extracellular CRF levels within the dlBNST (Fig. 2). One-way repeated-measures ANOVA demonstrated a significant effect of the formalin injection ($F_{(10,76)} = 4.50$, $p < 0.001$, $n = 7$). A significant increase in the CRF level was observed at 15–30 min after the formalin injection (186 ± 14%; $p < 0.01$ compared with the last baseline sample (–15 to 0 min), Newman–Keuls *post hoc* test).

Effects of intra-dlBNST injection of CRF receptor antagonists on formalin-induced CPA and nociceptive behaviors

To determine the role of CRF-mediated neurotransmission within the dlBNST in the affective component of pain, the effects of bilateral intra-dlBNST injection of NBI27914 (CRF_1 receptor antagonist) and AS-30 (CRF_2 receptor antagonist) on formalin-induced CPA were examined. In the intra-dlBNST vehicle-injected rats, the time spent in the pain-paired compartment during the test session (374 ± 33 and 391 ± 18 s in Fig. 3*A*,*B*, respectively) was significantly shorter ($t = 4.55$ (df = 6), $p < 0.01$ and $t = 4.91$ (df = 5), $p < 0.01$, respectively, paired *t* test) than the time during the preconditioning session (529 ± 19 and 538 ± 29 s). In the intra-dlBNST NBI27914 (0.3 and 1 nmol/side)-injected rats, no significant difference ($t = 2.19$ (df = 7), $p > 0.05$ and $t = 1.82$ (df = 6), $p > 0.05$, respectively, paired *t* test) was observed in the time spent in the pain-paired compartment between the test (480 ± 50 and 508 ± 41 s, respectively) and the preconditioning (551 ± 28 and 546 ± 32 s, respectively) sessions.

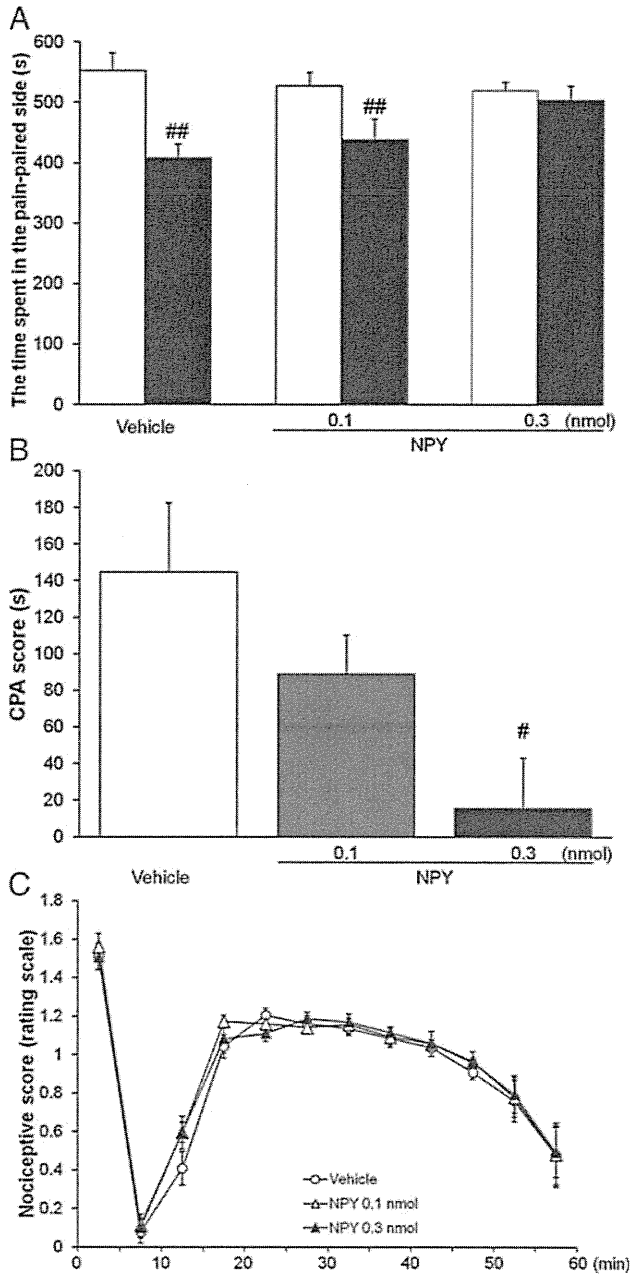

Figure 4. ***A, B***, Effects of intra-dlBNST injection of vehicle ($n = 8$) or NPY (0.1 nmol, $n = 7$; 0.3 nmol, $n = 7$) on formalin-induced CPA. Data are expressed as means ± SEM. The columns show the time spent in the pain-paired compartment in the preconditioning (white columns) and test (black columns) sessions (***A***). $^{\#\#}p < 0.01$ compared with the preconditioning session (paired *t* test). The columns show CPA scores (***B***). $^{\#}p < 0.05$ compared with vehicle-injected rats (Newman–Keuls *post hoc* test). ***C***, Effects of intra-dlBNST injection of vehicle ($n = 6$) or NPY (0.1 nmol, $n = 5$; 0.3 nmol, $n = 7$) on formalin-induced nociceptive behaviors. Data are expressed as means ± SEM.

Also, in the intra-dlBNST AS-30 (0.3 and 1 nmol/side)-injected groups, no significant difference ($t = 1.56$ (df = 5), $p > 0.05$ and $t = 1.51$ (df = 6), $p > 0.05$, respectively, paired *t* test) was observed in the time spent in the pain-paired compartment between the test (475 ± 20 and 502 ± 24 s, respectively) and the preconditioning (533 ± 32 and 535 ± 24 s, respectively) sessions. CPA scores showed dose-dependent attenuation of formalin-induced CPA by intra-dlBNST injection of these antagonists. As shown in Figure 3, *C* and *D*, one-way ANOVA indicated a significant

difference among groups (NBI27914, $F_{(2,19)} = 3.87$, $p < 0.05$ and AS-30, $F_{(2,16)} = 5.96$, $p < 0.05$). *Post hoc* comparisons revealed that NBI27914 at a dose of 1 nmol/side (37.6 ± 20.7 s; $p < 0.05$), but not 0.3 nmol/side (71.3 ± 32.5 s; $p > 0.05$), and AS-30 at doses of 0.3 and 1 nmol/side (58.3 ± 20.8 s, $p < 0.05$ and 33.3 ± 22.1 s, $p < 0.05$, respectively) attenuated formalin-induced CPA significantly compared with the vehicle-injected group (155 ± 34 s and 147 ± 30, respectively).

Because the dlBNST is located close to the lateral ventricle, it was possible that drugs leaking to the lateral ventricle might act on brain regions other than the dlBNST and suppress formalin-induced CPA. Thus, off-site control experiments were performed by injecting these antagonists into the lateral ventricle at a dose of 1 nmol/side. In the intracerebroventricularly injected NBI27914 and AS-30 groups ($n = 7$ each), the time spent in the pain-paired compartment during the test session (382 ± 23 and 452 ± 29 s, respectively) was significantly shorter ($t = 4.91$ (df = 6), $p < 0.01$ and $t = 3.61$ (df = 6), $p < 0.05$, respectively, paired t test) than the time during the preconditioning session (482 ± 8 and 535 ± 20 s, respectively). Thus, these results showed no suppressing effects of intracerebroventricularly administered NBI27914 and AS-30 on formalin-induced CPA, suggesting that the dlBNST was the likely site of action of these antagonists in suppressing formalin-induced CPA.

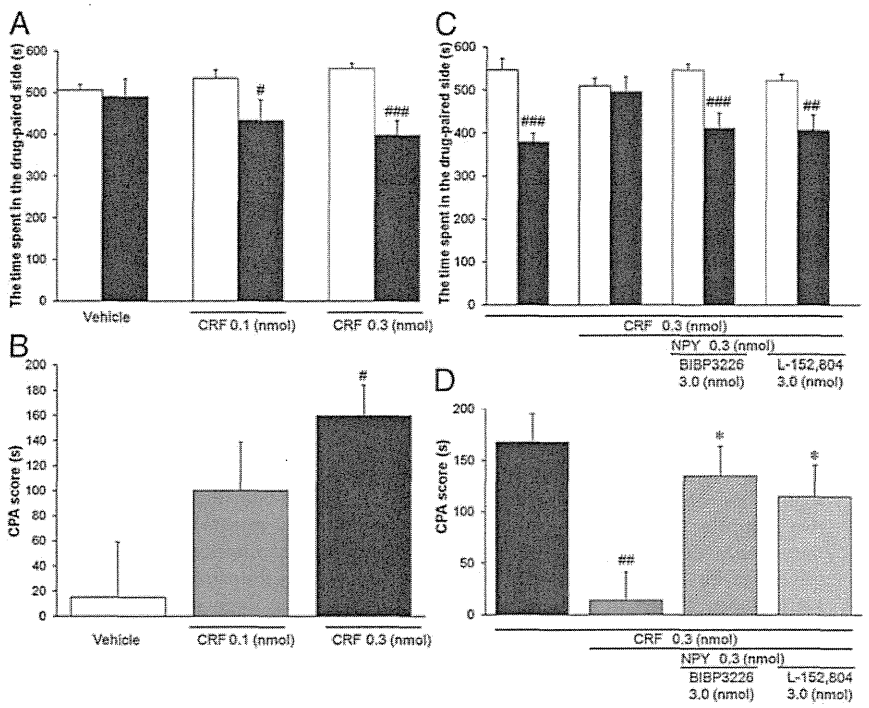

Figure 5. Effect of intra-dlBNST injection of NPY on CRF-induced CPA. ***A***, ***B***, Effects of intra-dlBNST injection of vehicle ($n = 10$) or CRF (0.1 nmol, $n = 10$; 0.3 nmol, $n = 11$) were examined using a place conditioning paradigm. Data are expressed as means ± SEM. ***A***, The columns show the time spent in the drug-paired compartment in the preconditioning (white columns) and test (black columns) sessions. #, ###$p < 0.05$, 0.001 compared with the preconditioning session (paired t test). ***B***, The columns show CPA scores. #$p < 0.05$ compared with vehicle-injected rats (Newman–Keuls *post hoc* test). ***C***, ***D***, Effects of intra-dlBNST injection of NPY in the presence or absence of subtype-selective NPY antagonists on CRF-induced CPA (CRF, $n = 10$; CRF + NPY, $n = 10$; CRF + NPY + BIBP3226, $n = 11$; CRF + NPY + L-152,804, $n = 12$). ***C***, The columns show the time spent in the drug-paired compartment in the preconditioning (white columns) and test (black columns) sessions. ##, ###$p < 0.01$, 0.001 compared with the preconditioning session (paired t test). ***D***, The columns show CPA scores. ##$p < 0.01$ compared with CRF alone-injected rats; *$p < 0.05$ compared with CRF + NPY-injected rats (Newman–Keuls *post hoc* test).

To examine whether intra-dlBNST injection of NBI27914 or AS-30 per se produced conditioned place preference (CPP) or CPA, these drugs (1 nmol/side) were injected into the bilateral dlBNST in the absence of intraplantar formalin injection. In both the intra-dlBNST NBI27914- and AS-30-injected groups ($n = 6$ and $n = 7$, respectively), no significant difference ($t = 1.06$ (df = 5), $p > 0.05$ and $t = 0.12$ (df = 6), $p > 0.05$, respectively, paired t test) was observed in the time spent in the drug-paired compartment between the test (491 ± 22 and 487 ± 33 s, respectively) and preconditioning (509 ± 28 and 491 ± 10 s, respectively) sessions. CPA scores were 18.3 ± 17.3 and 4.14 ± 33.5 s, respectively, which were not significantly different ($t = 0.21$ (df = 9), $p > 0.05$ and $t = 0.51$ (df = 11), $p > 0.05$, respectively, Student's t test) from the CPA score of the vehicle-injected group (23.8 ± 19.2 s, $n = 5$ and 28.7 ± 34.8 s, $n = 6$, respectively). These data showed that neither CPP nor CPA was induced by the intra-dlBNST injection of these antagonists, indicating that these drugs have no motivational effect by themselves when injected into the dlBNST at these doses.

As shown in Figure 3*E*, intra-dlBNST injection of NBI27914 (0.3 nmol/side or 1 nmol/side) or AS-30 (0.3 nmol/side or 1 nmol/side) did not affect formalin-induced nociceptive behaviors compared with the vehicle-injected group. Two-way repeated-measures ANOVA revealed no significant effect of these drugs ($F_{(4,31)} = 1.05$; $p > 0.05$) and no significant interaction between the drugs and time ($F_{(44,341)} = 0.89$; $p > 0.05$). These results showed that intra-dlBNST injection of neither NBI27914 nor AS-30 affected the sensory component of pain.

Effects of intra-dlBNST injection of NPY on formalin-induced CPA and nociceptive behaviors

The effects of intra-dlBNST injection of NPY (0.1 and 0.3 nmol/side) on formalin-induced CPA were examined. In the intra-dlBNST vehicle-injected and NPY (0.1 nmol/side)-injected groups, the time spent in pain-paired compartment during the test session (408 ± 23 and 438 ± 33 s, respectively) was significantly shorter ($t = 3.81$ (df = 7), $p < 0.01$ and $t = 4.20$ (df = 6), $p < 0.01$, respectively, paired t test) than the time during the preconditioning session (553 ± 29 and 527 ± 22 s, respectively; Fig. 4*A*). In the intra-dlBNST NPY (0.3 nmol/side)-injected group, no significant difference ($t = 0.57$ (df = 6), $p > 0.05$, paired t test) was observed in the time spent in the pain-paired compartment between the test (504 ± 24 s) and preconditioning (520 ± 13 s) sessions. CPA scores showed dose-dependent attenuation of formalin-induced CPA by intra-dlBNST injection of NPY (Fig. 4*B*). One-way ANOVA indicated a significant difference among groups ($F_{(2,19)} = 4.51$, $p < 0.05$). *Post hoc* comparisons revealed that NPY at a dose of 0.3 nmol/side (15.7 ± 27.3 s, $p < 0.05$), but not 0.1 nmol/side (89.0 ± 21.2 s), attenuated formalin-induced CPA significantly compared with the vehicle-injected group (145 ± 38.0 s).

The effects of off-site control injections of NPY (0.3 nmol/side) into the lateral ventricle on formalin-induced CPA were examined. In the intracerebroventricular NPY-injected group ($n = 7$), the time

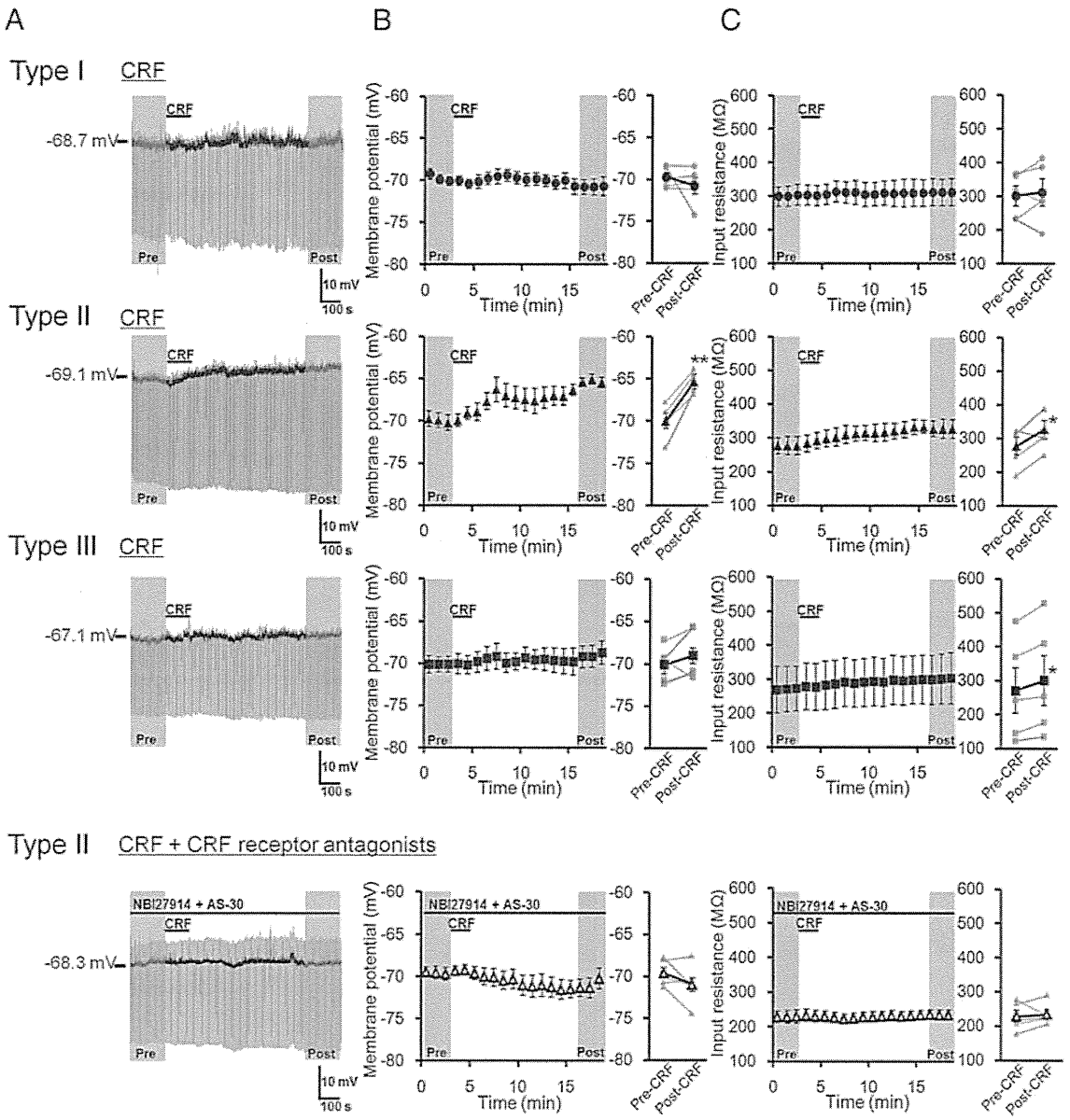

Figure 6. Effects of CRF on membrane potential and input resistance in three types of dlBNST neurons. ***A***, Representative traces from current-clamp recordings in type I (top), type II (second row), and type III (third row) dlBNST neurons, and type II dlBNST neurons in the presence of NBI27914 (300 nM) + AS-30 (300 nM) (bottom). ***B***, ***C***, Effects of CRF (1 μM, 2 min) on membrane potential (***B***) and input resistance (***C***) in type I ($n = 5$; top), type II ($n = 5$; second row), and type III ($n = 5$; third row) dlBNST neurons, and type II dlBNST neurons in the presence of NBI27914 + AS-30 ($n = 5$; bottom). Left, Time courses of membrane potential (***B***) and input resistance (***C***). Right, Averaged membrane potential (***B***) and input resistance (***C***) in the period of pre-CRF (0–3 min) and post-CRF (16–19 min) application. Gray symbols and lines show data obtained from individual neurons, and black symbols and lines show averaged data obtained from five neurons. Data are expressed as means ± SEM. $^*p < 0.05$, $^{**}p < 0.01$ compared with pre-CRF application (paired *t* test).

spent in the pain-paired compartment during the test session was 448 ± 30 s, which was significantly shorter ($t = 3.13$ (df = 6), $p < 0.05$, paired *t* test) than the time during the preconditioning session (553 ± 25 s). This result showed no suppressing effect of intracerebroventricularly administered NPY on formalin-induced CPA, suggesting that the dlBNST was the likely site of action of this peptide in suppressing formalin-induced CPA.

To examine whether intra-dlBNST injection of NPY per se produced CPP or CPA, NPY (0.3 nmol/side) was injected into the bilateral dlBNST in the absence of intraplantar formalin injection. In the intra-dlBNST NPY-injected group ($n = 5$), no significant difference ($t = 0.42$ (df = 4), $p > 0.05$, paired *t* test) was observed in the time spent in the drug-paired compartment between the test (501 ± 40 s) and preconditioning (488 ± 10 s) sessions. The CPA score (–13.4 ± 32.3 s) was not significantly different ($t = 0.09$ (df = 7), $p > 0.05$, Student's *t* test) from that of the vehicle-injected group (–18.3 ± 41.5 s, $n = 4$). These findings showed that neither CPP nor CPA was induced by the intra-dlBNST injection of NPY, indicating that this peptide has no motivational effect by itself when injected into the dlBNST at this dose.

As shown in Figure 4*C*, intra-dlBNST injection of NPY (0.1 nmol/side or 0.3 nmol/side) did not affect formalin-induced nociceptive behaviors compared with the vehicle-injected group. Two-way repeated-measures ANOVA revealed no significant effect of intra-dlBNST NPY ($F_{(2,15)} = 0.22$; $p > 0.05$) and no significant interaction between the drugs and time ($F_{(22,165)} = 0.48$; $p > 0.05$). These results showed that intra-dlBNST injection of NPY did not affect the sensory component of pain.

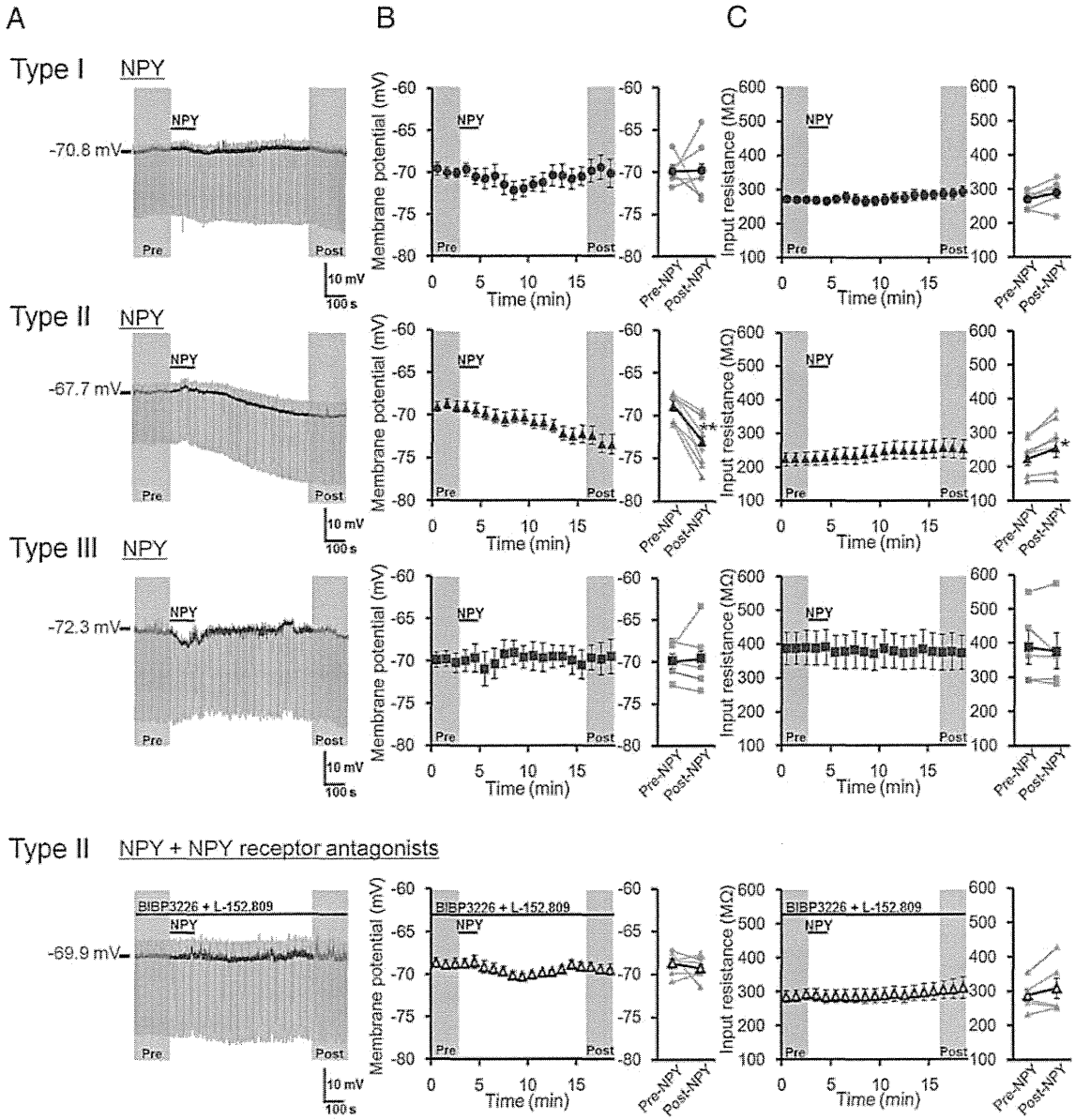

Figure 7. Effects of NPY on membrane potential and input resistance in three types of dlBNST neurons. ***A***, Representative traces from current-clamp recordings in type I (top), type II (second row), and type III (third row) dlBNST neurons, and type II dlBNST neurons in the presence of BIBP3226 (1 μM) + L-152,804 (1 μM) (bottom). ***B***, ***C***, Effects of NPY (1 μM, 2 min) on membrane potential (***B***) and input resistance (***C***) in type I ($n = 6$; top), type II ($n = 8$; second row), and type III ($n = 5$; third row) dlBNST neurons, and type II dlBNST neurons in the presence of BIBP3226 + L-152,804 ($n = 6$; bottom). Left, Time courses of membrane potential (***B***) and input resistance (***C***). Right, Averaged membrane potential (***B***) and input resistance (***C***) in the period of pre-NPY (0–3 min) and post-NPY (16–19 min) application. Gray symbols and lines show data obtained from individual neurons, and black symbols and lines show averaged data obtained from 5–8 neurons. Data are expressed as means ± SEM. *$p < 0.05$, **$p < 0.01$ compared with pre-NPY application (paired t test).

Effect of intra-dlBNST injection of NPY on CRF-induced CPA

Sahuque et al. (2006) reported that intra-BNST administration of CRF produced a dose-dependent CPA. First, we confirmed the induction of CPA by the intra-dlBNST injection of CRF. As shown in Figure 5*A*, in rats injected with CRF at doses of 0.1 and 0.3 nmol/side, the time spent in the drug-paired compartment during the test session (434 ± 49 and 399 ± 34 s, respectively) was significantly shorter ($t = 2.64$ (df = 9), $p < 0.05$ and $t = 6.50$ (df = 10), $p < 0.001$, respectively, paired t test) than the time during the preconditioning session (534 ± 21 and 558 ± 13 s, respectively). CPA scores revealed a dose-dependent induction of CPA by intra-dlBNST injection of CRF (Fig. 5*B*). One-way ANOVA indicated a significant difference among groups ($F_{(2,28)} = 4.15$, $p < 0.05$). *Post hoc* comparisons showed that CRF at a dose of 0.3 nmol/side (160 ± 25 s, $p < 0.05$), but not 0.1 nmol/side (99.4 ± 38.2 s, $p > 0.05$), significantly induced CPA compared with the vehicle-treated group (15.1 ± 44.1 s).

Next, the effect of coadministration of NPY on CRF-induced CPA was examined. In the rats simultaneously injected with CRF (0.3 nmol/side) and NPY (0.3 nmol/side), no significant difference ($t = 0.40$ (df = 9), $p > 0.05$, paired t test) was observed in the time spent in the drug-paired compartment between the test (496 ± 34 s) and preconditioning (510 ± 18 s) sessions (Fig. 5*C*). Coadministration of NPY with CRF significantly ($t = 3.43$ (df = 18), $p < 0.01$, Student's t test) reduced the CPA score (14.0 ± 35.3 s) compared with the CRF alone-injected group (167.7 ± 87.2 s; Fig. 5*D*).

To examine whether intra-dlBNST repeated injections of NPY per se produced CPP or CPA, NPY (0.3 nmol/side; $n = 6$)

was administered into the bilateral dlBNST in the absence of CRF over 3 d. No significant difference ($t = 0.48$ (df = 5), $p > 0.05$, paired t test) was observed in the time spent in the drug-paired compartment between the test (524 ± 19 s) and preconditioning (516 ± 21 s) sessions. The CPA score (−8.00 ± 16.8 s) was not significantly different ($t = 0.39$ (df = 14), $p > 0.05$, Student's t test) from that of the vehicle-injected group (15.1 ± 44.1 s, $n = 10$). These data showed that neither CPP nor CPA was induced by intra-dlBNST repeated injections of NPY alone, indicating that NPY had no motivational effect by itself when repeatedly injected into the dlBNST at this dose.

To identify the receptor subtype(s) involved in the inhibitory effect of NPY on CRF-induced CPA, the effects of coadministration of BIBP3226 (Y_1 selective antagonist) or L-152,804 (Y_5 selective antagonist) were examined. In the groups coadministered BIBP3226 (3.0 nmol/side) or L-152,804 (3.0 nmol/side) in addition to CRF and NPY, significant differences ($t = 4.68$ (df = 10), $p < 0.001$ or $t = 3.71$ (df = 11), $p < 0.01$, respectively, paired t test) were observed in the time spent in the drug-paired compartment between the test (412 ± 35 or 407 ± 35 s, respectively) and preconditioning (546 ± 16 or 521 ± 16 s, respectively) sessions (Fig. 5*C*). CPA scores of these groups (134 ± 29 or 114 ± 31 s, respectively) increased significantly ($t = 2.67$ (df = 19), $p < 0.05$ or $t = 2.15$ (df = 20), $p < 0.05$, respectively, Student's t test) compared with the score of the group injected with CRF and NPY (14.0 ± 35.3 s) (Fig. 5*D*).

Effects of CRF and NPY on membrane potentials in dlBNST neurons

Effects of CRF and NPY on the membrane potentials in dlBNST neurons were examined using a whole-cell patch-clamp technique in slice preparations. First, we examined the effects of a 2 min bath application of 1 μM CRF on membrane potentials in dlBNST neurons (Fig. 6). In type I neurons, CRF did not affect the membrane potential (−69.74 ± 0.55 and −70.76 ± 0.99 mV in the periods before and after CRF application, respectively; $t = 0.86$ (df = 4), $p > 0.05$, paired t test; Fig. 6*B*, top), and the input resistance was not changed (301.0 ± 29.5 and 311.4 ± 40.2 MΩ in the periods before and after CRF application, respectively; $t = 0.50$ (df = 4), $p > 0.05$, paired t test; Fig. 6*C*, top). On the other hand, CRF depolarized membrane potentials gradually in all of the type II neurons tested ($n = 5$). CRF application significantly changed the membrane potential from −69.97 ± 0.90 mV to −65.33 ± 0.56 mV ($t = 7.59$ (df = 4), $p < 0.01$, paired t test; Fig. 6*B*, second row). The input resistance in the postdrug period (327.0 ± 26.8 MΩ) was significantly higher than that in the predrug period (277.4 ± 26.0 MΩ; $t = 2.79$ (df = 4), $p < 0.05$, paired t test; Fig. 6*C*, second row). The CRF-induced depolarization and increase in input resistance were not observed in the presence of CRF receptor antagonists (300 nM NBI27914 + 300 nM AS-30), indicating that these changes were mediated by activation of CRF receptors (−69.59 ± 0.71 and −70.99 ± 1.10 mV before and after CRF application, respectively; $t = 1.66$ (df = 4), $p > 0.05$, paired t test; Fig. 6*B*, bottom; 228.9 ± 18.5 and 234.5 ± 14.3 MΩ before and after CRF application, respectively; $t = 0.41$ (df = 4), $p > 0.05$, paired t test; Figure 6*C*, bottom). Although CRF increased the input resistance in type III neurons slightly, but significantly (270.6 ± 67.0 and 300.5 ± 73.6 MΩ in the periods before and after CRF application, respectively; $t = 3.71$ (df = 4), $p < 0.05$, paired t test; Fig. 6*C*, third row), the membrane potential was not affected by CRF (−70.14 ± 0.95 and −69.05 ± 1.35 mV in the periods before and after CRF application, respectively; $t = 1.20$ (df = 4), $p > 0.05$, paired t test; Fig. 6*A*,*B*, third row) in this type of neurons.

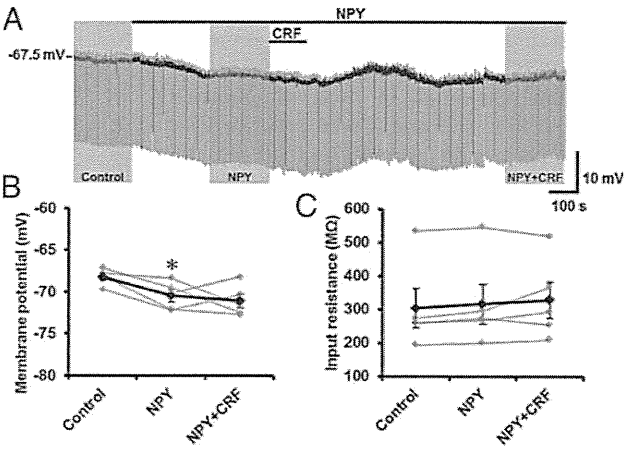

Figure 8. Inhibitory effects of NPY on CRF-induced depolarization in type II dlBNST neurons. ***A***, Representative trace from current-clamp recording in a type II dlBNST neuron. The effects of the peptides were evaluated in the periods indicated by shading (Control, 0–3 min before NPY application; NPY, 0–3 min before CRF application; NPY + CRF, 12–15 min after CRF application). ***B***, ***C***, Effects of CRF on membrane potential (***B***) and input resistance (***C***) in the presence of NPY. Gray symbols and lines show data obtained from individual neurons ($n = 5$), and black symbols and lines show averaged data obtained from five neurons. *$p < 0.05$ compared with control (Newman–Keuls *post hoc* test).

Next, we investigated the effects of a 2 min bath application of 1 μM NPY on the membrane potentials in dlBNST neurons (Fig. 7). In type I neurons, NPY did not affect either the membrane potential (−69.89 ± 0.66 and −69.78 ± 1.44 mV in the periods before and after NPY application, respectively; $t = 0.06$ (df = 5), $p > 0.05$, paired t test; Fig. 7*A*,*B*, top), and the input resistance (270.2 ± 10.1 and 288.5 ± 16.4 MΩ in the periods before and after NPY application, respectively; $t = 1.82$ (df = 5), $p > 0.05$, paired t test; Fig. 7*C*, top). On the other hand, NPY hyperpolarized membrane potentials gradually in all of the type II neurons tested ($n = 8$). NPY application significantly changed membrane potential from −68.91 ± 0.59 to −73.05 ± 1.06 mV ($t = 5.39$ (df = 7), $p < 0.01$, paired t test; Fig. 7*B*, second row). The input resistance in the postdrug period (254.9 ± 28.5 MΩ) was significantly larger than that in the predrug period (223.7 ± 19.5 MΩ; $t = 3.15$ (df = 7), $p < 0.05$, paired t test; Fig. 7*C*, second row). In the presence of NPY receptor antagonists (1 μM BIBP3226 + 1 μM L-152,804), NPY did not affect either the membrane potentials (−68.75 ± 0.56 and −69.35 ± 0.56 mV before and after NPY application, respectively; $t = 0.82$ (df = 5), $p > 0.05$, paired t test; Fig. 7*B*, bottom) or the input resistance (287.5 ± 16.9 and 307.9 ± 28.9 MΩ before and after NPY application, respectively; $t = 1.41$ (df = 5), $p > 0.05$, paired t test; Fig. 7*C*, bottom), suggesting that the effects of NPY were mediated via NPY receptors. In type III neurons, NPY did not affect either the membrane potential (−69.94 ± 0.96 and −69.61 ± 1.77 mV in the periods before and after NPY application, respectively; $t = 0.29$ (df = 4), $p > 0.05$, paired t test; Fig. 7*B*, third row) or the input resistance (387.8 ± 49.2 and 376.2 ± 52.5 MΩ in the periods before and after NPY application, respectively; $t = 0.68$ (df = 4), $p > 0.05$, paired t test; Fig. 7*C*, third row).

The opposing effects of CRF and NPY on the membrane potential in type II dlBNST neurons allowed us to examine the effects of NPY on CRF-induced depolarization (Fig. 8). As seen in Figure 8, *A* and *B*, in type II neurons, significant hyperpolarization was observed after NPY application (−68.20 ± 0.43 and −70.46 ± 0.75 mV in the periods before and after NPY application, respectively; $p < 0.05$, compared with the pre-application of drugs (Control), one-way repeated measured ANOVA ($F_{(2,8)} =$

4.83, $p < 0.05$) with Bonferroni's *post hoc* test, $n = 5$;Figure 8*B*). In the presence of NPY, CRF did not depolarize the membrane potential in type II neurons (–70.46 ± 0.75 and –71.06 ± 0.83 mV in the periods before and after CRF application, respectively; Fig. 8*B*). We occasionally observed a transient excitation after CRF application in the presence of NPY (Fig. 8*A*). However, the depolarization was very small and did not persist over ~16 min, where CRF usually exhibits maximal depolarization in the absence of NPY. The input resistance was also unaltered by CRF in the presence of NPY (316.1 ± 59.8 and 328.0 ± 54.3 MΩ in the periods before and after CRF application, respectively; Fig. 8*C*).

Conductances associated with the actions of CRF and NPY in type II dlBNST neurons

To investigate the conductances underlying the actions of CRF and NPY, we studied the effects of these peptides on the steady-state *I–V* relationships in type II neurons by applying a voltage ramp protocol. As shown in Figure 9, *A* and *B*, CRF-induced net currents in individual neurons were heterogeneous: CRF decreased net currents in some neurons ($n = 4$, Fig. 9*A*, left, *B*, black traces), while the increase in net currents was observed in other neurons ($n = 6$; Fig. 9*A*, right, *B*, gray traces). Thus, we classified these neurons into two groups and designated them as type IIa and type IIb. The averaged current trace of type IIa neurons revealed that the reversal potential of this current was approximately –95 mV (–94.4 ± 3.9 mV, $n = 4$), which is close to the potassium equilibrium potential (–109.3 mV) calculated from the Nernst equation under our experimental conditions (Fig. 9*C*, left). On the other hand, the CRF-induced increased currents reversed the polarity at approximately –50 mV (–55.9 ± 6.1 mV, $n = 6$) with a clear outward rectification in type IIb neurons, suggesting a contribution of nonselective cationic conductance (Takano et al., 1996; Yang and Ferguson, 2002; Murai and Akaike, 2005; Kaneko et al., 2008) (Fig. 9*C*, right). CRF significantly increased negative holding currents (–58.92 ± 8.54 and –67.77 ± 9.63 pA before and after CRF application, respectively; $t = 2.80$ (df = 9), $p < 0.05$, paired *t* test; Fig. 9*D*, upper), whereas the input resistance was not affected by CRF (339.9 ± 36.3 and 342.5 ± 39.1 MΩ before and after CRF application, respectively; $t = 0.31$ (df = 9), $p > 0.05$, paired *t* test; Fig. 9*D*, lower). These results suggest that at least two conductances might be associated with the CRF-induced depolarization. We observed the different effects of CRF on changes in input resistance between voltage- and current-clamp recordings. Voltage-clamp recordings were obtained from four type IIa and six type IIb neurons, which exhibited increased and decreased input resistance after CRF application, respectively. Thus, the apparent net change in input resistance seemed to be unchanged. On the other hand, in current-clamp recordings (Fig. 6), averaged input resistance was increased following CRF application. Although we did not determine the cell classes (IIa or IIb) in the current-clamp recording experiment, based on the changes in input resistance observed in individual neurons, it might be possible that the recorded neurons included four type IIa and one type IIb neurons.

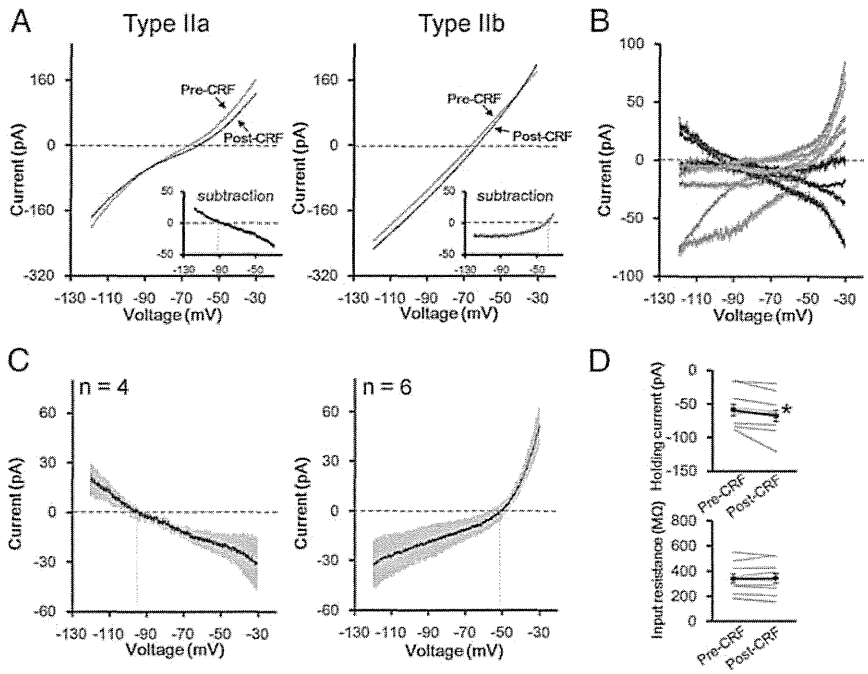

Figure 9. Conductances associated with the action of CRF in the type II dlBNST neurons. ***A***, Representative steady-state current responses to voltage ramp pulses from –30 to –120 mV recorded from type IIa (left) and type IIb (right) neurons in the periods of pre-CRF (gray) and post-CRF (black) application (1 μM, 2 min). The insets show the subtraction of the currents (CRF-induced net currents). Axis titles in ***A*** apply in the insets. ***B***, Traces of CRF-induced net currents in four type IIa (black) and six type IIb (gray) neurons. ***C***, Average traces of CRF-induced currents in type IIa ($n = 4$, left) and type IIb ($n = 6$, right) neurons. Gray shadows represent SEM. Vertical dashed lines show the reversal potential. ***D***, Effects of CRF on the holding currents at –70 mV (upper) and the input resistance (lower). Gray lines represent the data obtained from individual neurons ($n = 10$), and black symbols and lines show the averaged data obtained from 10 neurons. $^*p < 0.05$ compared with pre-CRF application (paired *t* test).

On the other hand, NPY-induced net currents in individual neurons were similar in all of the neurons tested: NPY decreased net currents in all recorded neurons ($n = 8$, Fig. 10*A*,*B*). This result suggests that type II neurons cannot be classified according to the response to NPY. In other words, both type IIa and IIb neurons may respond to NPY in the same manner. NPY-induced change in the net currents was accompanied by significantly reduced negative holding currents (–62.64 ± 10.06 and –54.81 ± 10.12 pA before and after NPY application, respectively; $t = 4.05$ (df = 7), $p < 0.01$, paired *t* test; Fig. 10*C*, upper) and increased input resistance (304.3 ± 30.3 and 359.9 ± 48.6 MΩ before and after NPY application, respectively; $t = 2.37$ (df = 7), $p < 0.05$, paired *t* test; Fig. 10*C*, lower). The averaged trace exhibited that the current associated with NPY reversed the polarity approximately –60 mV (–60.4 ± 6.0 mV, $n = 8$; Fig. 10*B*), suggesting a contribution of multiple conductances to the action of NPY. One of the candidate conductances is hyperpolarization-activated current (I_h), the suppression of which has been shown to be critical for NPY-induced hyperpolarization in the BLA (Giesbrecht et al., 2010). Thus, we tested this hypothesis by using I_h blocker ZD7288 (Fig. 10*D–F*). Bath application of 10 μM ZD7288 alone elicited significant hyperpolarizing currents (–31.72 ± 8.62 and –11.43 ± 6.70 pA in the periods 0–3 min before and 7–10 min after ZD7288 application, respectively; $t = 3.66$ (df = 7), $p < 0.01$, paired *t* test, $n = 8$) and increased input resistance (482.21 ± 36.7 and 744.9 ± 124.6 MΩ in the periods 0–3 min before and 7–10 min after ZD7288 application, respectively; $t =$

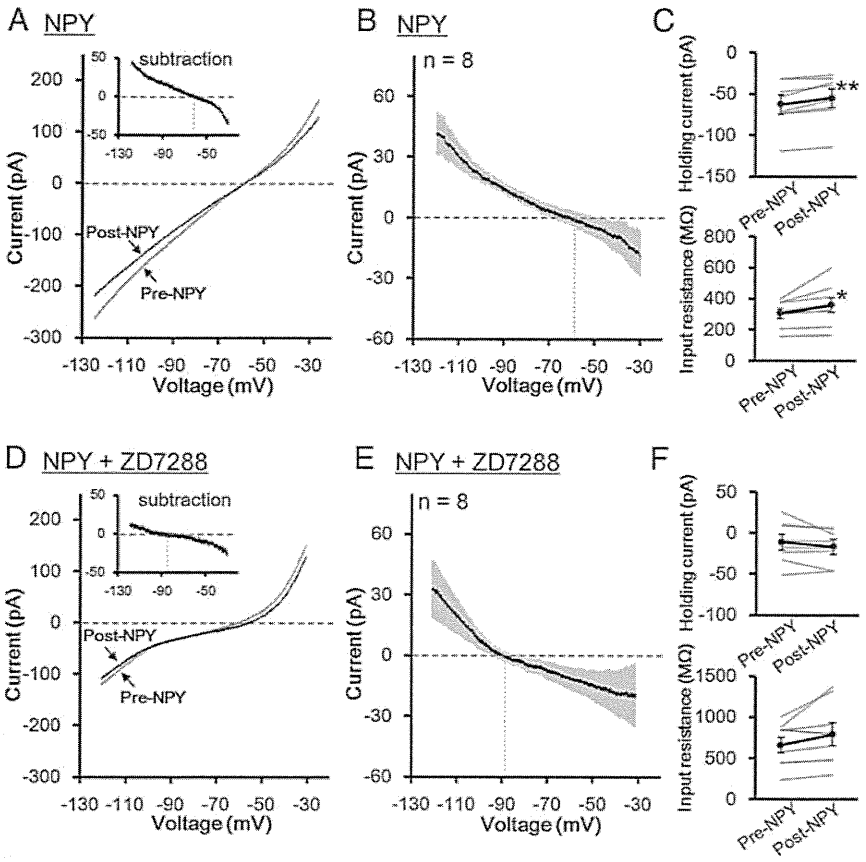

Figure 10. Conductances associated with the action of NPY in the type II dlBNST neurons. ***A***, ***D***, Representative steady-state current responses to voltage ramp pulses from −30 to −120 mV recorded from type II neurons in the periods of pre-NPY (gray) and post-NPY (black) (1 μM, 2 min) application in the absence (***A***) or presence (***D***) of ZD7288 (10 μM). The insets show the subtraction of the currents (NPY-induced net currents). Axis titles in ***A*** and ***D*** apply in the insets. ***B***, ***E***, Average traces of NPY-induced currents in type II neurons in the absence (***B***; $n = 8$) or presence (***E***; $n = 8$) of ZD7288. Gray shadows represent SEM. Vertical dashed lines show the reversal potential. ***C***, ***F***, Effects of NPY on the holding currents at −70 mV (upper) and the input resistance (lower). Gray lines represent the data obtained from individual neurons, and black symbols and lines show the averaged data obtained from eight neurons. $^*p < 0.05$, $^{**}p < 0.01$ compared with pre-NPY application (paired *t* test).

2.75 (df = 7), $p < 0.05$, paired *t* test, $n = 8$), indicating that I_h constitutively depolarizes membrane potentials in type II neurons. In the presence of ZD7288, NPY did not affect either the holding currents (−11.07 ± 8.92 and −16.54 ± 7.40 pA before and after NPY application, respectively; $t = 1.47$ (df = 7), $p > 0.05$, paired *t* test; Fig. 10*F*, upper) or the input resistance (662.9 ± 95.8 and 791.8 ± 183.9 MΩ before and after NPY application, respectively; $t = 2.05$ (df = 7), $p > 0.05$, paired *t* test; Fig. 10*F*, lower). In the presence of ZD7288, the reversal potential of NPY-associated currents shifted to a more negative potential (−85.3 ± 6.2 mV, $n = 8$; Fig. 10*E*) compared with the reversal potential in the absence of ZD7288 (−60.4 ± 6.0 mV). These results indicate that NPY-induced hyperpolarization was mediated primarily by suppression of I_h in type II dlBNST neurons. The remaining ZD7288-resistant component, which showed a negative slope conductance with the reversal potential of approximately −85 mV, might be mediated, at least in part, by closing potassium channels.

Effects of CRF and NPY on the firing activity in type II dlBNST neurons

The effects of CRF and NPY on the firing activity in type II dlBNST neurons were examined. A 2 min bath application of 1 μM CRF gradually depolarized membrane potentials, as observed in the above experiments, and then induced spikes (Fig. 11*A*), which persisted over 30 min. The number of spikes significantly increased from 12.2 ± 7.1 spikes/1.5 min in the period before CRF application to 206.8 ± 68.1 spikes/1.5 min in the period after CRF application ($t = 3.35$ (df = 5), $p < 0.05$, $n = 6$, paired *t* test; Fig. 11*B*). On the other hand, NPY tended to suppress the firing activity (Fig. 11*C*). The number of spikes decreased from 28.5 ± 26.5 in the period before NPY application to 15.0 ± 12.3 spikes/1.5 min in the period during NPY application (Fig. 11*D*). In the presence of NPY, no significant increase in the spikes was observed after the application of 1 μM CRF (35.8 ± 30.8 spikes/1.5 min; $t = 0.21$ (df = 5), $p > 0.05$ vs control (before NPY application) and $t = 0.62$ (df = 5), $p > 0.05$ vs NPY alone (during NPY application), $n = 6$, paired *t* test; Figure 11*D*).

Discussion

In the current study, using a conditioned place paradigm and an *in vivo* microdialysis technique, we demonstrated that enhanced neurotransmission via CRF receptors within the dlBNST plays a key role in the negative affective component of pain. Additionally, we showed that intra-dlBNST injection of NPY suppressed pain-induced CPA. To our knowledge, these findings are the first reported providing evidence of the opposing roles of CRF and NPY within the dlBNST in the negative affective component of pain. We also demonstrated that intra-dlBNST CRF injection produced CPA even in the absence of formalin-evoked noxious stimulation and that coadministration of NPY suppressed CRF-induced CPA. These results suggest that NPY injected into the dlBNST may suppress formalin-induced CPA through inhibition of CRF-mediated neurotransmission.

Behavioral studies using a CPA test have successfully elucidated the neural substrates and mechanisms underlying the affective component of pain (Johansen et al., 2001; Tanimoto et al., 2003; Deyama et al., 2008). Because this test was based on associative learning between a noxious stimulus-induced aversive affect and a neutral environmental context, whether the attenuation of CPA was due to impairment of associative learning or suppression of the primary aversive affect is difficult to determine. In the present study, we demonstrated that intra-dlBNST CRF injection produced CPA even in the absence of formalin-induced noxious stimulus. This indicates that the activation of CRF receptors within the dlBNST is sufficient to produce the negative affective states. Therefore, the attenuation of CPA by inhibition of intra-dlBNST CRF-mediated neurotransmission may be due to the reduction of the primary aversive affect.

To investigate the cellular mechanisms of CRF-induced CPA and the counteracting effect of NPY, we examined the effects of CRF and NPY on neuronal excitability in dlBNST neurons. Interestingly, we found that only type II, not type I or III, neurons responded to both CRF and NPY in the dlBNST. Bath application of CRF depolarized

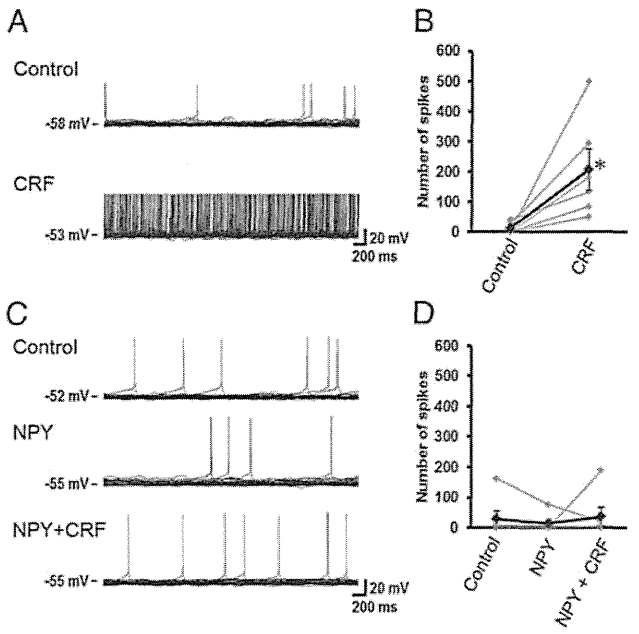

Figure 11. Effects of CRF on firing activity of type II dlBNST neurons in the absence (***A***, ***B***; $n = 6$) and presence (***C***, ***D***; $n = 6$) of NPY. ***A***, ***C***, Representative traces (36 overlaid) from current-clamp recordings in type II dlBNST neurons before and after application of peptides. ***B***, ***D***, Effects of CRF and NPY on the number of spikes in type II dlBNST neurons. Gray symbols and lines show data obtained from individual neurons, and black symbols and lines show averaged data obtained from six neurons. $*p < 0.05$ compared with pre-CRF application control (paired *t* test).

membrane potentials significantly in type II neurons. In contrast, NPY-induced hyperpolarization in type II neurons. Additionally, coapplication of NPY extinguished the CRF-induced depolarization. Similar results were observed in firing activities of type II dlBNST neurons. Specifically, CRF increased firing activities of type II neurons significantly, and coapplication of NPY suppressed them. These results demonstrated opposing effects of CRF and NPY at the cellular level, as observed at the behavioral level. These counteracting effects of CRF and NPY on neuronal excitability in type II dlBNST neurons may explain the opposing roles of these peptides in the negative affective component of pain.

Analyses of *I–V* relationships in the absence and presence of CRF demonstrate that there may be at least two classes of type II dlBNST neurons. The steady-state current in type IIa neurons was reduced by CRF and reversed its polarity at approximately –95 mV, suggesting the involvement of potassium channels. Jedema and Grace (2004) reported the direct action of CRF on locus ceruleus neurons, increasing neuronal excitability by decreasing a potassium conductance in a cAMP-dependent manner. A similar mechanism may be involved in the depolarizing effect of CRF on type IIa dlBNST neurons. On the other hand, CRF increased steady-state current and its reversal potential was approximately –50 mV in type IIb neurons, implying the contribution of nonselective cation current (Takano et al., 1996; Yang and Ferguson, 2002; Kaneko et al., 2008). In support of this hypothesis, CRF has been reported to activate nonselective cationic conductances in the pituitary grand (Takano et al., 1996). The reversal potentials observed in the type IIa and IIb neurons were slightly deviated from the predicted (–109.3 mV for potassium current) or reported (>–45 mV for nonselective cation current) (Takano et al., 1996; Ito and Dulon, 2002; Yang and Ferguson, 2002; Kaneko et al., 2008) values, suggesting that both channels express in both type IIa and IIb neurons with different levels, rather each channel exclusively expresses in either type IIa or IIb neurons. Further studies are necessary to characterize the detailed physiological properties of these two types of neurons.

NPY hyperpolarized type II dlBNST neurons with an increase in input resistance. *I–V* relationship analyses revealed that NPY reduced steady-state currents, the reversal potential of which was approximately –60 mV, indicating suppression of cationic conductance(s). Consistent with this finding, ZD7288, an I_h blocker, inhibited the hyperpolarizing effect of NPY and shifted the reversal potential of NPY-associated currents toward a more negative potential, demonstrating that NPY-induced hyperpolarization was mediated by blocking I_h channels. Similar hyperpolarizing effect of NPY via inhibition of I_h channels has been reported in BLA pyramidal neurons (Giesbrecht et al., 2010).

A previous study suggested that the majority of type II BNST neurons were GABAergic interneurons, which may innervate output neurons within the BNST (Hammack et al., 2007). Thus, CRF-induced activation of type II neurons could result in the inhibition of output neurons. Indeed, in the ventrolateral BNST, Dumont and Williams (2004) demonstrated that activation of neurons exhibiting a depolarizing sag (type I or II neurons) enhanced $GABA_A$-IPSC in the output neurons projecting to the ventral tegmental area (VTA). Georges and Aston-Jones (2001, 2002) have reported that the BNST sends excitatory drive to VTA dopaminergic neurons. Recently, we have demonstrated that this excitatory drive from the BNST to VTA dopaminergic neurons is mainly composed of two GABAergic neurons (Kudo et al., 2012). Specifically, most VTA-projecting BNST neurons are GABAergic neurons, which preferentially innervate VTA GABAergic neurons. Therefore, activation of VTA-projecting BNST output neurons is predicted to promote VTA dopaminergic neuron activity through a disinhibition mechanism. Pain-induced increase in CRF release within the BNST may activate the type II BNST neurons, which could suppress VTA-projecting BNST output neurons, thereby attenuating the excitatory drive from the BNST to the VTA dopaminergic neurons. The attenuation of VTA dopaminergic neuron activity through this mechanism may be involved in pain-induced aversion. In support of this hypothesis, it has recently been reported that optogenetic inhibition of VTA dopaminergic neurons causes CPA (Tan et al., 2012).

Although several lines of evidence suggest the critical role of CRF_1 receptors in CRF-induced negative emotion such as anxiety and fear, there is still continued controversy over the role of CRF_2 receptors in these emotional states (Takahashi, 2001; Bale and Vale, 2004). Regarding the BNST, Sahuque et al. (2006) reported that anxiety-like behaviors induced by the intra-BNST CRF injection were prevented by coadministration of a CRF_1, but not a CRF_2, receptor antagonist. On the other hand, either CRF_1 or CRF_2 receptor antagonist prevented CPA induced by intra-BNST CRF injection, consistent with our current results showing that both CRF_1 and CRF_2 receptor antagonists suppressed pain-induced CPA. These findings suggest that distinct neuronal pathways may be involved in different negative emotional states such as anxiety and aversion. Further studies using neuronal pathway-specific methods such as optogenetic approaches are necessary to address this issue.

A large body of literature suggests that anxiolytic and anti-aversive effects of NPY are mediated primarily by Y_1 receptors (Heilig, 1995; Kask et al., 1997; Nakajima et al., 1998; Primeaux et al., 2005). Additionally, there are reports that Y_5 receptors also mediate the suppression of negative affect (Sørensen et al., 2004). In contrast, Y_2 receptors have been reported to mediate negative emotions, such

as anxiety (Nakajima et al., 1998; Sajdyk et al., 2002). Thus, in the present study, we examined the involvement of Y_1 and Y_5 subtypes in the inhibitory effect of intra-dlBNST NPY on CRF-induced CPA and found that both Y_1 and Y_5 receptors play important roles in this effect of NPY. In this study, we revealed the heterogeneity of type II dlBNST neurons. Further electrophysiological experiments using Y_1- and Y_5-specific agonists are needed to clarify the neuronal populations expressing these receptors.

Increasing data have demonstrated opposing effects of CRF and NPY. Intracerebroventricular injection of Y_1 receptor antagonist BIBP3226 induced an anxiogenic effect in the elevated plus maze test in rats, which was blocked by pretreatment with a nonselective CRF receptor antagonist (Kask et al., 1997). Sajdyk et al. (2006) reported that urocortin I, a CRF receptor agonist, injected into the BLA-induced CPA, which was reversed by coadministration of NPY. Electrophysiological analysis revealed opposing actions of CRF and NPY on the excitability of BLA neurons (Giesbrecht et al., 2010). In the ventrolateral BNST, it has been reported that NPY and CRF have opposite modulating effects on $GABA_A$-IPSC (Kash and Winder, 2006). The present study has added pain-induced aversion to the list of negative emotional states in which opposing effects of CRF and NPY play important roles.

Further studies are necessary to determine the neuronal circuits involved in the induction of negative affect associated with pain stimulation, and the molecular mechanisms operating the ion channels involved in the opposing actions of CRF and NPY on dlBNST neuronal excitability. Nevertheless, we have uncovered some of the neuronal mechanisms underlying the negative affective component of pain by showing the opposing roles of intra-dlBNST CRF and NPY in pain-induced aversive behaviors and the opposing actions of these peptides on neuronal excitability converging on the same target, type II neurons, within the dlBNST.

References

Bale TL, Vale WW (2004) CRF and CRF receptors: role in stress responsivity and other behaviors. Annu Rev Pharmacol Toxicol 44:525–557. CrossRef Medline

Deyama S, Nakagawa T, Kaneko S, Uehara T, Minami M (2007) Involvement of the bed nucleus of the stria terminalis in the negative affective component of visceral and somatic pain in rats. Behav Brain Res 176:367–371. CrossRef Medline

Deyama S, Katayama T, Ohno A, Nakagawa T, Kaneko S, Yamaguchi T, Yoshioka M, Minami M (2008) Activation of the β-adrenoceptor-protein kinase A signaling pathway within the ventral bed nucleus of the stria terminalis mediates the negative affective component of pain in rats. J Neurosci 28:7728–7736. CrossRef Medline

Deyama S, Katayama T, Kondoh N, Nakagawa T, Kaneko S, Yamaguchi T, Yoshioka M, Minami M (2009) Role of enhanced noradrenergic transmission within the ventral bed nucleus of the stria terminalis in visceral pain-induced aversion in rats. Behav Brain Res 197:279–283. CrossRef Medline

Deyama S, Ide S, Kondoh N, Yamaguchi T, Yoshioka M, Minami M (2011) Inhibition of noradrenaline release by clonidine in the ventral bed nucleus of the stria terminalis attenuates pain-induced aversion in rats. Neuropharmacology 61:156–160. CrossRef Medline

Dumont EC, Williams JT (2004) Noradrenaline triggers $GABA_A$ inhibition of bed nucleus of the stria terminalis neurons projecting to the ventral tegmental area. J Neurosci 24:8198–8204. CrossRef Medline

Georges F, Aston-Jones G (2001) Potent regulation of midbrain dopamine neurons by the bed nucleus of the stria terminalis. J Neurosci 21:RC160. Medline

Georges F, Aston-Jones G (2002) Activation of ventral tegmental area cells by the bed nucleus of the stria terminalis: a novel excitatory amino acid input to midbrain dopamine neurons. J Neurosci 22:5173–5187. Medline

Giesbrecht CJ, Mackay JP, Silveira HB, Urban JH, Colmers WF (2010) Countervailing modulation of I_h by neuropeptide Y and corticotrophin-releasing factor in basolateral amygdala as a possible mechanism for their effects on stress-related behaviors. J Neurosci 30:16970–16982. CrossRef Medline

Gutman AR, Yang Y, Ressler KJ, Davis M (2008) The role of neuropeptide Y in the expression and extinction of fear-potentiated startle. J Neurosci 28:12682–12690. CrossRef Medline

Hammack SE, Mania I, Rainnie DG (2007) Differential expression of intrinsic membrane currents in defined cell types of the anterolateral bed nucleus of the stria terminalis. J Neurophysiol 98:638–656. CrossRef Medline

Hara Y, Nakaya H (1997) Dual effects of extracellular ATP on the muscarinic acetylcholine receptor-operated K^+ current in guinea-pig atrial cells. Eur J Pharmacol 324:295–303. CrossRef Medline

Heilig M (1995) Antisense inhibition of neuropeptide Y (NPY)-Y_1 receptor expression blocks the anxiolytic-like action of NPY in amygdala and paradoxically increases feeding. Regul Pept 59:201–205. CrossRef Medline

Ito K, Dulon D (2002) Nonselective cation conductance activated by muscarinic and purinergic receptors in rat spiral ganglion neurons. Am J Physiol Cell Physiol 282:C1121–1135. Medline

Jedema HP, Grace AA (2004) Corticotropin-releasing hormone directly activates noradrenergic neurons of the locus ceruleus recorded *in vitro*. J Neurosci 24:9703–9713. CrossRef Medline

Johansen JP, Fields HL (2004) Glutamatergic activation of anterior cingulate cortex produces an aversive teaching signal. Nat Neurosci 7:398–403. CrossRef Medline

Johansen JP, Fields HL, Manning BH (2001) The affective component of pain in rodents: direct evidence for a contribution of the anterior cingulate cortex. Proc Natl Acad Sci U S A 98:8077–8082. CrossRef Medline

Kaneko K, Tamamaki N, Owada H, Kakizaki T, Kume N, Totsuka M, Yamamoto T, Yawo H, Yagi T, Obata K, Yanagawa Y (2008) Noradrenergic excitation of a subpopulation of GABAergic cells in the basolateral amygdala via both activation of nonselective cationic conductance and suppression of resting K^+ conductance: a study using glutamate decarboxylase 67-green fluorescent protein knock-in mice. Neuroscience 157:781–797. CrossRef Medline

Kash TL, Winder DG (2006) Neuropeptide Y and corticotropin-releasing factor bi-directionally modulate inhibitory synaptic transmission in the bed nucleus of the stria terminalis. Neuropharmacology 51:1013–1022. CrossRef Medline

Kask A, Rägo L, Harro J (1997) Alpha-helical CRF(9–41) prevents anxiogenic-like effect of NPY Y_1 receptor antagonist BIBP3226 in rats. Neuroreport 8:3645–3647. CrossRef Medline

Kosten TA (1994) Clonidine attenuates conditioned aversion produced by naloxone-precipitated opiate withdrawal. Eur J Pharmacol 254:59–63. CrossRef Medline

Kudo T, Uchigashima M, Miyazaki T, Konno K, Yamasaki M, Yanagawa Y, Minami M, Watanabe M (2012) Three types of neurochemical projection from the bed nucleus of the stria terminalis to the ventral tegmental area in adult mice. J Neurosci 32:18035–18046. CrossRef Medline

Lee Y, Davis M (1997) Role of the hippocampus, the bed nucleus of the stria terminalis, and the amygdala in the excitatory effect of corticotropin-releasing hormone on the acoustic startle reflex. J Neurosci 17:6434–6446. Medline

Morin SM, Ling N, Liu XJ, Kahl SD, Gehlert DR (1999) Differential distribution of urocortin- and corticotropin-releasing factor-like immunoreactivities in the rat brain. Neuroscience 92:281–291. CrossRef Medline

Murai Y, Akaike T (2005) Orexins cause depolarization via nonselective cationic and K^+ channels in isolated locus coeruleus neurons. Neurosci Res 51:55–65. CrossRef Medline

Nakagawa T, Yamamoto R, Fujio M, Suzuki Y, Minami M, Satoh M, Kaneko S (2005) Involvement of the bed nucleus of the stria terminalis activated by the central nucleus of the amygdala in the negative affective component of morphine withdrawal in rats. Neuroscience 134:9–19. CrossRef Medline

Nakajima M, Inui A, Asakawa A, Momose K, Ueno N, Teranishi A, Baba S, Kasuga M (1998) Neuropeptide Y produces anxiety via Y2-type receptors. Peptides 19:359–363. CrossRef Medline

Parker RM, Herzog H (1999) Regional distribution of Y-receptor subtype mRNAs in rat brain. Eur J Neurosci 11:1431–1448. CrossRef Medline

Paxinos G, Watson C (1998) The rat brain in stereotaxic coordinates, Ed 4. San Diego, CA: Academic.

Primeaux SD, Wilson SP, Cusick MC, York DA, Wilson MA (2005) Effects

of altered amygdalar neuropeptide Y expression on anxiety-related behaviors. Neuropsychopharmacology 30:1589–1597. CrossRef Medline

Rafieian-Kopaei M, Gray AM, Spencer PS, Sewell RD (1995) Contrasting actions of acute or chronic paroxetine and fluvoxamine on morphine withdrawal-induced place conditioning. Eur J Pharmacol 275:185–189. CrossRef Medline

Sahuque LL, Kullberg EF, Mcgeehan AJ, Kinder JR, Hicks MP, Blanton MG, Janak PH, Olive MF (2006) Anxiogenic and aversive effects of corticotropin-releasing factor (CRF) in the bed nucleus of the stria terminalis in the rat: role of CRF receptor subtypes. Psychopharmacology 186: 122–132. CrossRef Medline

Sajdyk TJ, Schober DA, Smiley DL, Gehlert DR (2002) Neuropeptide Y-Y_2 receptors mediate anxiety in the amygdala. Pharmacol Biochem Behav 71:419–423. CrossRef Medline

Sajdyk TJ, Fitz SD, Shekhar A (2006) The role of neuropeptide Y in the amygdala on corticotropin-releasing factor receptor-mediated behavioral stress responses in the rat. Stress 9:21–28. CrossRef Medline

Sakanaka M, Shibasaki T, Lederis K (1986) Distribution and efferent projections of corticotropin-releasing factor-like immunoreactivity in the rat amygdaloid complex. Brain Res 382:213–238. CrossRef Medline

Sørensen G, Lindberg C, Wörtwein G, Bolwig TG, Woldbye DP (2004) Differential roles for neuropeptide Y Y_1 and Y_5 receptors in anxiety and sedation. J Neurosci Res 77:723–729. CrossRef Medline

Takahashi LK (2001) Role of CRF_1 and CRF_2 receptors in fear and anxiety. Neurosci Biobehav Rev 25:627–636. CrossRef Medline

Takano K, Yasufuku-Takano J, Teramoto A, Fujita T (1996) Corticotropin-releasing hormone excites adrenocorticotropin-secreting human pituitary adenoma cells by activating a nonselective cation current. J Clin Invest 98:2033–2041. CrossRef Medline

Tan KR, Yvon C, Turiault M, Mirzabekov JJ, Doehner J, Labouèbe G, Deisseroth K, Tye KM, Lüscher C (2012) GABA neurons of the VTA drive conditioned place aversion. Neuron 73:1173–1183. CrossRef Medline

Tanimoto S, Nakagawa T, Yamauchi Y, Minami M, Satoh M (2003) Differential contributions of the basolateral and central nuclei of the amygdala in the negative affective component of chemical somatic and visceral pains in rats. Eur J Neurosci 18:2343–2350. CrossRef Medline

Tzschentke TM (1998) Measuring reward with the conditioned place preference paradigm: a comprehensive review of drug effects, recent progress and new issues. Prog Neurobiol 56:613–672. CrossRef Medline

Van Pett K, Viau V, Bittencourt JC, Chan RK, Li HY, Arias C, Prins GS, Perrin M, Vale W, Sawchenko PE (2000) Distribution of mRNAs encoding CRF receptors in brain and pituitary of rat and mouse. J Comp Neurol 428:191–212. CrossRef Medline

Walter A, Mai JK, Lanta L, Görcs T (1991) Differential distribution of immunohistochemical markers in the bed nucleus of the stria terminalis in the human brain. J Chem Neuroanat 4:281–298. CrossRef Medline

Yang B, Ferguson AV (2002) Orexin-A depolarizes dissociated rat area postrema neurons through activation of a nonselective cationic conductance. J Neurosci 22:6303–6308. Medline

Progress in Neuro-Psychopharmacology & Biological Psychiatry 39 (2012) 107–111

Contents lists available at SciVerse ScienceDirect

Progress in Neuro-Psychopharmacology & Biological Psychiatry

journal homepage: www.elsevier.com/locate/pnp

The effects of the co-administration of the α_1-adrenoreceptor antagonist prazosin on the anxiolytic effect of citalopram in conditioned fear stress in the rat

Naoki Takamura [a,b], Takahiro Masuda [a,b], Takeshi Inoue [a,*], Shin Nakagawa [a], Tsukasa Koyama [a]

[a] Department of Psychiatry, Hokkaido University Graduate School of Medicine, Sapporo, Japan
[b] Pharmacology Research Laboratories, Dainippon Sumitomo Pharma Co., Ltd., Osaka, Japan

ARTICLE INFO

Article history:
Received 20 February 2012
Received in revised form 10 May 2012
Accepted 23 May 2012
Available online 30 May 2012

Keywords:
Anxiety
Conditioned fear
Prazosin
Selective serotonin reuptake inhibitor

ABSTRACT

Several studies have shown that the α_1-adrenoreceptor is involved in controlling extracellular serotonin levels. The administration of the α_1-adrenoreceptor antagonist prazosin was shown to decrease extracellular serotonin levels in the hippocampus, the prefrontal cortex and the raphe nucleus, while the administration of the α_1-adrenoreceptor agonist cirazoline was shown to increase serotonin levels. Furthermore, the elevation of serotonin levels induced by the selective serotonin reuptake inhibitor (SSRI) citalopram was attenuated by prazosin. Thus, α_1-adrenoreceptor antagonists may affect SSRI-induced increases in extracellular serotonin levels and their antidepressive and anxiolytic effects. However, little is known about the influence of α_1-adrenoreceptor antagonists on the behavioral pharmacological effects of SSRIs. The conditioned fear stress-induced freezing behavior is an animal model of anxiety and can detect the anxiolytic effect of SSRIs. To clarify whether an α_1-adrenoreceptor antagonist affects the anxiolytic action of SSRIs, we examined the effects of the co-administration of the α_1-adrenoreceptor antagonist prazosin and the SSRI citalopram using the contextual conditioned fear stress model. Low-dose prazosin (0.03 mg/kg) significantly attenuated the citalopram (3 mg/kg)-induced decrease in conditioned freezing. Moreover, high-dose (0.5 mg/kg), but not low-dose (0.03 mg/kg), prazosin significantly attenuated citalopram (10 mg/kg)-induced decreases in conditioned freezing. These drugs did not affect the spontaneous motor activity of the rats. Therefore, these results suggest that blocking the α_1-adrenoreceptor decreases the anxiolytic effect of citalopram.

1. Introduction

Selective serotonin reuptake inhibitors (SSRIs) are prescribed for many disorders, including major depressive disorder and various anxiety disorders (generalized anxiety disorder, panic disorder, post-traumatic stress disorder, *etc.*) (Zohar and Westenberg, 2000). Brain microdialysis studies have shown that SSRIs increase the extracellular serotonin concentrations 2–5 fold in the raphe nucleus, the hypothalamus and the cerebral cortex (Fuller, 1994). These long-term changes in extracellular serotonin concentrations induce receptor reorganization, hippocampal neurogenesis and other changes (Santarelli et al., 2003; Stahl, 1998). These changes are thought to be relevant to the efficacy of SSRIs in depressive and anxiety disorders.

Several *in vivo* brain microdialysis studies suggest that the α_1-adrenoreceptor is involved in controlling extracellular serotonin levels. The administration of prazosin, a selective and centrally active α_1-adrenoreceptor antagonist (Menkes et al., 1981), was shown to decrease extracellular serotonin levels in the hippocampus, the prefrontal cortex and the raphe nucleus (Gobert et al., 1998; Hjorth et al., 1995; Pudovkina et al., 2003; Rouquier et al., 1994). Conversely, the administration of the α_1-adrenoreceptor agonist cirazoline increased extracellular serotonin levels in the raphe nucleus (Amargos-Bosch et al., 2005; Pudovkina et al., 2003). The elevation of serotonin levels induced by citalopram in the raphe nucleus, the prefrontal cortex and the hippocampus was attenuated by the concurrent administration of prazosin (Rea et al., 2010).

Furthermore, antipsychotic drugs, which are used as augmentation therapy for treatment-resistant depression and anxiety disorders, and most tricyclic antidepressants have α_1-adrenoreceptor antagonistic effects (Bandelow et al., 2008; Gillman, 2007; Lam et al., 2009; Leysen et al., 1993; Nasrallah, 2008; Richelson and Souder, 2000). Earlier studies have shown that the antipsychotic drug olanzapine, which has a significant affinity for the α_1-adrenoreceptor, attenuated the increase in extracellular serotonin levels induced by fluoxetine (an SSRI) as measured by *in vivo* microdialysis studies (Koch et al., 2004; Zhang et al., 2000). This result suggests that these α_1-adrenoreceptor antagonistic drugs affect SSRI-induced increases in extracellular serotonin levels and therefore modulate their antidepressant and anxiolytic effects. However, little is known

Abbreviations: ANOVA, analysis of variance; SSRI, selective serotonin reuptake inhibitor; SERT, serotonin transporter; NET, norepinephrine transporter.

* Corresponding author at: Department of Psychiatry, Hokkaido University Graduate School of Medicine, North 15, West 7, Sapporo 060-8638, Japan. Tel.: +81 11 706 5160; fax: +81 11 706 5081.
E-mail address: tinoue@med.hokudai.ac.jp (T. Inoue).

0278-5846/$ – see front matter © 2012 Elsevier Inc. All rights reserved.
doi:10.1016/j.pnpbp.2012.05.017

about the influence of α_1-adrenoreceptor antagonists on the behavioral pharmacological effects of SSRIs.

The conflict test and the elevated plus-maze test are generally used as animal models of anxiety to evaluate the efficacy of benzodiazepines, a class of anxiolytic drugs. However, these traditional animal models of anxiety failed to demonstrate the anxiolytic effect of SSRIs (Borsini et al., 2002). Thus, it has proven difficult to study the mechanism of anxiolytic actions of SSRIs using these animal models. The conditioned fear stress-induced freezing model can be used as an animal model of anxiety. Our previous studies have shown that the freezing behavior is attenuated by both benzodiazepines and serotonergic anxiolytic drugs, including serotonin1A receptor agonists and SSRIs (Hashimoto et al., 1996; Inoue et al., 1996, 2004, 2011; Nishitsuji et al., 2006). Thus, the conditioned fear stress model is thought suitable to evaluate drugs affecting serotonergic neurotransmission. Based on our previous studies, SSRIs are thought to mitigate anxiety in the contextual conditioned fear stress model by increasing extracellular serotonin levels by blocking the serotonin transporter and enhancing serotonergic neural transmission (Inoue et al., 2011). Taken together with the previous studies described above concerning the role of α_1-adrenoreceptors in controlling serotonin release, it is hypothesized that the α_1-adrenoreceptor antagonists interfere with the effect of SSRIs on the conditioned fear stress-induced freezing behavior by inhibiting the increase in extracellular serotonin levels effected by SSRIs.

In this study, to verify the hypothesis that antagonism of the α_1-adrenoreceptor affects the anxiolytic action of SSRIs, we examined the effects of the co-administration of the α_1-adrenoreceptor antagonist prazosin with the SSRI citalopram in the contextual conditioned fear stress model. These results showed that the α_1-adrenoreceptor antagonist prazosin attenuated the inhibitory effects of citalopram on conditioned freezing. In addition, this effect was independent of any non-specific effects on motor activity. These results suggest that α_1-adrenoreceptors play an important role in SSRI-induced anxiolytic effects on conditioned fear in rats.

2. Methods

2.1. Animals

Male Sprague–Dawley rats (250–350 g) were obtained from the Shizuoka Laboratory Animal Center (Shizuoka, Japan). The rats were housed in groups of four in a temperature-controlled environment (22 ± 1 °C) with free access to food and water. The subjects were maintained on a 12 h light/dark cycle (light phase: 06:30–18:30). The experiments began after a 1 week acclimatization period. The rats were tested between 08:30 and 11:30.

All experiments were approved by the Hokkaido University School of Medicine Animal Care and Use Committee and were in compliance with the Guide for the Care and Use of Laboratory Animals.

2.2. Drugs

Citalopram hydrobromide was donated by the Dainippon Sumitomo Pharma Co., Ltd. Prazosin hydrochloride was obtained from the Sigma-Aldrich Corp. (St. Louis, MO, USA). Citalopram was dissolved in 0.9% NaCl solution (saline) and administered by subcutaneous injection (s.c.) at a volume of 1 ml/kg 60 min prior to testing. Prazosin was dissolved in 0.5% methylcellulose and administered by intraperitoneal injection (i.p.) at a volume of 1 ml/kg 75 min prior to testing. The doses of citalopram and prazosin used in this study were based on our previous experiments and previous reports by other investigators (Inoue et al., 2011; Kakui et al., 2009; Rouquier et al., 1994; Selken and Nichols, 2007).

2.3. The contextual conditioned fear stress model

The rats were individually subjected to 150 s of inescapable electric footshock (five 2.5 mA scramble footshocks, pulse wave, 30 s duration) that were delivered at intershock intervals of 35–80 s (mean 60 s) in a shock chamber with a grid floor ($19 \times 22 \times 20$ cm, Medical Agent Co., Kyoto, Japan). The electric shocks were applied by a Model SGS-02D Shock Generator (Medical Agent Co.). A day later, the rats were placed in the shock chamber without any footshock and observed for 5 min. Their behavior was videotaped and later scored by human observation. During the observation period (test period), the duration of freezing behavior was recorded using a modified time-sampling procedure, as previously described (Inoue et al., 2004). Every 10 s, the behavior in which the subject was currently engaged was classified as either 'freezing' or 'activity'. Freezing was defined as the absence of any observable movement of the skeleton and the vibrissae, except that related to respiration. All other behavior was scored as activity. The subject was classified as either freezing or active according to its behavior throughout the entire 10-s period.

The percentage scores for the duration of freezing behavior (% freezing) were calculated for each 5-min observation period.

2.4. The assay of motor activity

To exclude the possibility that citalopram and prazosin administration affect freezing nonspecifically by affecting spontaneous activity, we measured rat spontaneous activity for 5 min, the same period used to monitor conditioned freezing. In detail, the motor activity of unshocked rats was measured after the administration of prazosin (0.03 and 0.5 mg/kg, i.p.), citalopram (3 and 10 mg/kg, s.c.) and after the co-administration of both drugs. The rats were individually habituated in their home cages to the testing room for one day. Prazosin was administrated 75 min prior to testing, and citalopram was administered 60 min prior to testing. Rats were individually placed in a testing cage. Their motor activity was automatically recorded for 5 min as previously described by Ohmori et al. (1994) using an infrared sensor that detected thermal radiation. Horizontal movement was responsible for most of the count. Other body movements also contributed when they included a substantial horizontal component.

2.5. Data analysis

All data are presented as the mean ± SEM of the individual values for each rat among the groups. Statistical analyses of the freezing behavior and motor activity data were performed using a one-way analysis of variance (ANOVA) followed by a Fisher's LSD test for parametric multiple comparisons. In the event that the data were not normally distributed or homogenous for variance, a Kruskal–Wallis analysis followed by a Scheffe test for non-parametric analyses was performed to detect any significant effects of treatments.

3. Results

3.1. The effect of the co-administration of prazosin (0.03 mg/kg) with acute low-dose citalopram (3 mg/kg) treatment on conditioned freezing

The SSRI citalopram (3 mg/kg) significantly reduced the duration of conditioned freezing. Although the administration of prazosin (0.03 mg/kg) by itself effected no remarkable change in conditioned freezing, the co-administration of prazosin reversed the freezing inhibition induced by citalopram [$F(3, 56) = 4.12$, $P<0.05$, one-way-ANOVA] (Fig. 1).

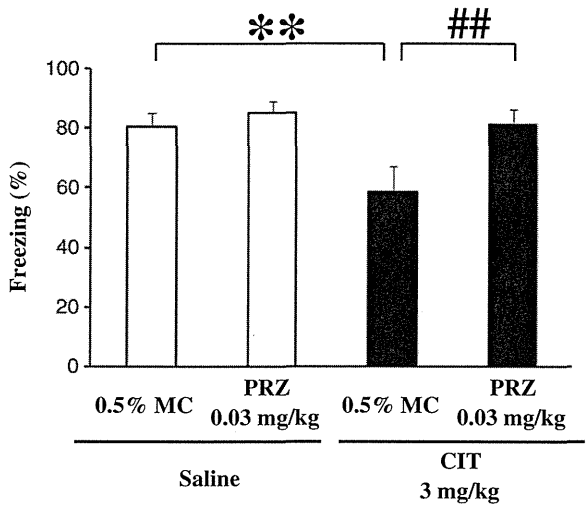

Fig. 1. The effect of the co-administration of prazosin with acute low-dose citalopram treatment (3 mg/kg) on conditioned fear in rats. One day after footshocks, vehicle or prazosin (PRZ; 0.03 mg/kg, i.p.) and saline or citalopram (CIT; 3 mg/kg, s.c.) were administered 75 min and 60 min before testing, respectively. The data are presented as the mean ± SEM (n = 14–16). **P<0.01 versus vehicle control and ##P<0.01 versus citalopram alone (Fisher's PLSD test). MC, methylcellulose.

3.2. The effect of the co-administration of prazosin (0.03 mg/kg and 0.5 mg/kg) with acute high-dose citalopram (10 mg/kg) treatment on conditioned freezing

We next investigated the effect of prazosin (0.03 mg/kg) on the high-dose citalopram (10 mg/kg)-induced anxiolytic effect. Citalopram (10 mg/kg) alone significantly reduced the conditioned freezing response. However, prazosin (0.03 mg/kg) failed to antagonize the citalopram-induced inhibition of freezing behavior [F (3, 28) = 4.50, P<0.05, one-way ANOVA] (Fig. 2a). Because 0.03 mg/kg prazosin did not antagonize the anxiolytic effect of citalopram (10 mg/kg) (Fig. 2a), we next investigated whether 0.5 mg/kg of prazosin affected the anxiolytic effect of citalopram (10 mg/kg). While the administration of prazosin (0.5 mg/kg) alone did not affect conditioned freezing, the co-administration of prazosin completely reversed the anxiolytic effect of citalopram (10 mg/kg) [H = 13.20, P<0.01, Kruskal–Wallis test] (Fig. 2b).

3.3. Motor activity

Citalopram and prazosin had no effect on the motor activity of the rats. Furthermore, the co-administration of prazosin and citalopram also had no effect on locomotor activities (Table 1).

4. Discussion

In the present study, the α_1-adrenoreceptor antagonist prazosin attenuated the inhibitory effects of citalopram on conditioned freezing. Prazosin itself had no effect on conditioned freezing. The administration of citalopram alone, prazosin alone or their combination did not influence rat locomotor activities. Therefore, the effect of the co-administration of citalopram and prazosin on conditioned freezing was likely not due to non-specific effects on motor activities. Thus, these results suggest the importance of the α_1-adrenoreceptor in the citalopram-induced anxiolytic effect in the rat contextual conditioned fear model.

SSRIs increase extracellular serotonin levels by binding to serotonin transporters and suppressing serotonin reuptake (Fuller, 1994). While SSRIs do not exhibit an anxiolytic effect in traditional anxiety models such as the conflict test or the elevated plus maze (Borsini et al., 2002), our previous studies showed that the SSRIs exhibited an anxiolytic effect in the conditioned fear stress-induced freezing model consistent with clinical findings that SSRIs are effective in the treatment of anxiety disorders; we also showed that the increase in extracellular serotonin levels induced by SSRIs decreases conditioned freezing (Inoue et al., 2011). Thus, this model is suitable to evaluate the mechanism of the anxiolytic effect of SSRIs, and the results from this model may be extrapolated to human anxiety disorders with the consideration of some limitations.

Previous investigations have demonstrated that noradrenergic neurons project to the dorsal raphe nucleus and the serotonergic neurons in the raphe nucleus are under the α_1-adrenoreceptor-mediated tonic facilitatory influence (Baraban and Aghajanian, 1980, 1981; Lejeune et al., 1994; Vandermaelen and Aghajanian, 1983). Therefore, changes in the noradrenergic activities of the raphe nucleus may modulate the serotonergic neurotransmission in several brain regions relevant to anxiety, including the frontal cortex, the hippocampus and the amygdala. In fact, α_1-adrenoreceptor antagonists suppress the firing activity of serotonergic neurons in the raphe nucleus (Lejeune et al., 1994; Vandermaelen and Aghajanian, 1983), and serotonin release was inhibited by antagonizing

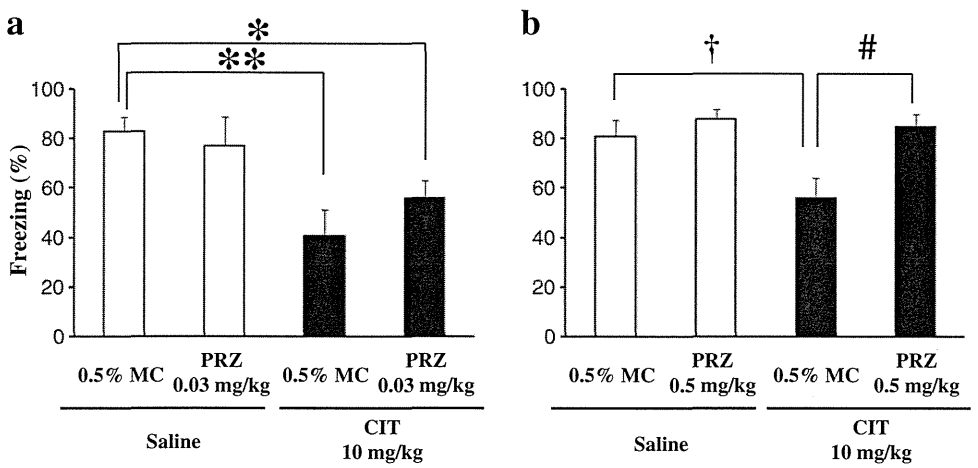

Fig. 2. The effect of the co-administration of prazosin with acute high-dose citalopram treatment (10 mg/kg, i.p.) on conditioned fear in rats. (a) Vehicle or prazosin (PRZ; 0.03 mg/kg, i.p.) and saline or citalopram (CIT; 10 mg/kg, s.c.) were administered 75 min and 60 min before testing, respectively. (b) Vehicle or prazosin (PRZ; 0.5 mg/kg, i.p.) and saline or citalopram (CIT; 10 mg/kg, s.c.) were administered 75 min and 60 min before testing, respectively. The data are presented as the mean ± SEM (n = 16) (a) *P<0.05, **P<0.01 versus vehicle control (Fisher's PLSD test), (b) †P<0.05 versus vehicle control and #P<0.05 versus citalopram alone (Scheffe test).

Table 1
The effect of the co-administration of prazosin (PRZ; 0.03 mg/kg or 0.5 mg/kg) and citalopram (CIT; 3 mg/kg or 10 mg/kg) on spontaneous motor activity.

Drug treatment (mg/kg)	Motor activity (counts/5 min)
0.5% MC + saline	10.4 ± 8.7
PRZ (0.03) + saline	0 ± 0
0.5% MC + CIT (3)	4.0 ± 2.6
PRZ (0.03) + CIT (3)	9.8 ± 6.7
0.5% MC + saline	15.3 ± 9.1
PRZ (0.5) + saline	2.1 ± 1.9
0.5% MC + CIT (10)	24.5 ± 8.6
PRZ (0.5) + CIT (10)	1.1 ± 0.8

All data are represented as the mean ± SEM (n = 8). MC, methylcellulose.

the α_1-adrenoreceptors of the rat hippocampus, the prefrontal cortex and the raphe nucleus (Gobert et al., 1998; Hjorth et al., 1995; Pudovkina et al., 2003; Rouquier et al., 1994). Moreover, citalopram increased extracellular serotonin levels in the raphe nucleus, the prefrontal cortex and the hippocampus that was attenuated by the co-administration of prazosin (Rea et al., 2010). Citalopram has a selectively high affinity for the serotonin transporter (SERT) and low affinity for the norepinephrine transporter (NET) and various monoamine receptors including the α_1-adrenoreceptor (Millan et al., 2001). Moreover, the doses of citalopram used in the present study significantly increased extracellular serotonin levels but do not significantly affect the extracellular levels of noradrenaline or dopamine (Bymaster et al., 2002; Millan et al., 2001). Thus, our results were not caused by a direct effect of prazosin on citalopram-induced changes in noradrenergic neural transmission. Taken together with the previous studies, our results support the hypothesis that α_1 antagonism attenuates serotonin release, thereby interfering with the anxiolytic effect of SSRIs on conditioned freezing.

In this study, low-dose prazosin (0.03 mg/kg) failed to attenuate the anxiolytic effect of high-dose citalopram (10 mg/kg). However, high-dose prazosin (0.5 mg/kg) attenuated the anxiolytic effect of high-dose citalopram (10 mg/kg) (Fig. 2). Rouquier et al. (1994) showed that systemic administration of prazosin at doses of 0.03, 0.1 and 0.4 mg/kg [intravenous injection (i.v.)] decreased the extracellular serotonin levels in the rat hippocampus in a dose-dependent manner (50%, 60% and 65%, respectively, 60 min after drug administration). They also showed that the systemic administration of 0.4 mg/kg (i.v.) prazosin decreased the extracellular serotonin levels (a 35% decrease 60 min after administration) in the striatum, although 0.03 mg/kg prazosin did not affect serotonin release. Therefore, it can be concluded that high-dose prazosin (0.5 mg/kg) was necessary to inhibit the anxiolytic effect of high-dose citalopram (10 mg/kg). Our data support this conclusion because high-dose prazosin (0.5 mg/kg) is more potent at inhibiting serotonin release than low-dose prazosin (0.03 mg/kg). Thus, these results suggest that the more antagonistic a drug is toward the α_1-adrenoreceptor, the more potently the drug attenuates the anxiolytic effect of SSRIs.

Earlier *in vivo* microdialysis studies examining the co-administration of an antipsychotic drug (with an affinity for α_1-adrenoreceptors) and SSRIs support a role for α_1-adrenoreceptors in the modulation of extracellular serotonin levels. The acute administration of the atypical antipsychotic drug olanzapine attenuated the increase in extracellular serotonin induced by fluoxetine (Koch et al., 2004; Zhang et al., 2000). These results might be explained by the affinity of olanzapine for the α_1-adrenoreceptor. The results of our study and previous studies by other investigators suggest that the use of α_1-adrenoreceptor antagonists in conjunction with SSRIs may weaken the clinical efficacy of the SSRIs. Clinically, such α_1 antagonistic types of antidepressants and antipsychotics are widely used to treat depressive and anxiety disorders (Bandelow et al., 2008; Lam et al., 2009). Our results suggest that we should consider whether the drugs to be coprescribed with SSRIs are α_1-aderenoreceptor antagonists because such drugs may attenuate the antidepressive and anxiolytic effects of SSRIs.

Clinically, however, SSRIs exhibit their antidepressive and anxiolytic effects only after long-term treatment (Den Boer and Westenberg, 1988; Oehrberg et al., 1995). Thus, we next plan to examine the chronic effect of prazosin and citalopram co-administration in future experiments. Moreover, we also plan to investigate the efficacy of the combined administration of various antipsychotics and SSRIs on conditioned freezing. The results of these further studies may provide useful information to guide clinical anti-anxiety therapy.

5. Conclusion

In conclusion, the findings of this study show that prazosin attenuates the citalopram-induced anxiolytic effect. This study demonstrates that the citalopram-induced suppression of freezing in the conditioned freezing model was significantly attenuated by the administration of the α_1-adrenoreceptor antagonist prazosin. Antagonists of the α_1-adrenoreceptor may play an important role in SSRI-induced anxiolytic effects on conditioned fear in rats.

Conflicts of interest

Dr. Tsukasa Koyama has received honoraria from GlaxoSmithKline, Astellas and Eli Lilly and has received research/grant support from Dainippon Sumitomo Pharma, Astellas and GlaxoSmithKline; he is a member of the advisory board of GlaxoSmithKline and Mitsubishi Tanabe Pharma. The other authors declare that they have no conflicts of interest.

Acknowledgments

This work was supported in part by Grants-in-Aid for Scientific Research No. 21591478 (T. Inoue) from the Japanese Ministry of Education, Culture, Sports, Science and Technology.

References

Amargos-Bosch M, Artigas F, Adell A. Effects of acute olanzapine after sustained fluoxetine on extracellular monoamine levels in the rat medial prefrontal cortex. Eur J Pharmacol 2005;516:235–8.
Bandelow B, Zohar J, Hollander E, Kasper S, Moller HJ, Allgulander C, et al. World Federation of Societies of Biological Psychiatry (WFSBP) guidelines for the pharmacological treatment of anxiety, obsessive-compulsive and post-traumatic stress disorders — first revision. World J Biol Psychiatry 2008;9:248–312.
Baraban JM, Aghajanian GK. Suppression of firing activity of 5-HT neurons in the dorsal raphe by alpha-adrenoceptor antagonists. Neuropharmacology 1980;19:355–63.
Baraban JM, Aghajanian GK. Noradrenergic innervation of serotonergic neurons in the dorsal raphe: demonstration by electron microscopic autoradiography. Brain Res 1981;204:1-11.
Borsini F, Podhorna J, Marazziti D. Do animal models of anxiety predict anxiolytic-like effects of antidepressants? Psychopharmacology 2002;163:121–41.
Bymaster FP, Zhang W, Carter PA, Shaw J, Chernet E, Phebus L, et al. Fluoxetine, but not other selective serotonin uptake inhibitors, increases norepinephrine and dopamine extracellular levels in prefrontal cortex. Psychopharmacology (Berl) 2002;160:353–61.
Den Boer JA, Westenberg HG. Effect of a serotonin and noradrenaline uptake inhibitor in panic disorder; a double-blind comparative study with fluvoxamine and maprotiline. Int Clin Psychopharmacol 1988;3:59–74.
Fuller RW. Uptake inhibitors increase extracellular serotonin concentration measured by brain microdialysis. Life Sci 1994;55:163–7.
Gillman PK. Tricyclic antidepressant pharmacology and therapeutic drug interactions updated. Br J Pharmacol 2007;151:737–48.
Gobert A, Rivet JM, Audinot V, Newman-Tancredi A, Cistarelli L, Millan MJ. Simultaneous quantification of serotonin, dopamine and noradrenaline levels in single frontal cortex dialysates of freely-moving rats reveals a complex pattern of reciprocal auto- and heteroreceptor-mediated control of release. Neuroscience 1998;84:413–29.
Hashimoto S, Inoue T, Koyama T. Serotonin reuptake inhibitors reduce conditioned fear stress-induced freezing behavior in rats. Psychopharmacology (Berl) 1996;123: 182–6.
Hjorth S, Bengtsson HJ, Milano S, Lundberg JF, Sharp T. Studies on the role of 5-HT1A autoreceptors and alpha 1-adrenoceptors in the inhibition of 5-HT release—I. BMY7378 and prazosin. Neuropharmacology 1995;34:615–20.
Inoue T, Hashimoto S, Tsuchiya K, Izumi T, Ohmori T, Koyama T. Effect of citalopram, a selective serotonin reuptake inhibitor, on the acquisition of conditioned freezing. Eur J Pharmacol 1996;311:1–6.
Inoue T, Kitaichi Y, Koyama T. SSRIs and conditioned fear. Prog Neuropsychopharmacol Biol Psychiatry 2011;35:1810–9.
Inoue T, Li XB, Abekawa T, Kitaichi Y, Izumi T, Nakagawa S, et al. Selective serotonin reuptake inhibitor reduces conditioned fear through its effect in the amygdala. Eur J Pharmacol 2004;497:311–6.

Kakui N, Yokoyama F, Yamauchi M, Kitamura K, Imanishi T, Inoue T, et al. Anxiolytic-like profile of mirtazapine in rat conditioned fear stress model: functional significance of 5-hydroxytryptamine 1A receptor and α_1-adrenergic receptor. Pharmacol Biochem Behav 2009;92:393–8.

Koch S, Perry KW, Bymaster FP. Brain region and dose effects of an olanzapine/fluoxetine combination on extracellular monoamine concentrations in the rat. Neuropharmacology 2004;46:232–42.

Lam RW, Kennedy SH, Grigoriadis S, McIntyre RS, Milev R, Ramasubbu R, et al. Canadian Network for Mood and Anxiety Treatments (CANMAT) clinical guidelines for the management of major depressive disorder in adults. III. Pharmacotherapy. J Affect Disord 2009;117(Suppl. 1):S26–43.

Lejeune F, Audinot V, Gobert A, Rivet JM, Spedding M, Millan MJ. Clozapine inhibits serotoninergic transmission by an action at alpha 1-adrenoceptors not at 5-HT1A receptors. Eur J Pharmacol 1994;260:79–83.

Leysen JE, Janssen PM, Schotte A, Luyten WH, Megens AA. Interaction of antipsychotic drugs with neurotransmitter receptor sites *in vitro* and *in vivo* in relation to pharmacological and clinical effects: role of 5HT2 receptors. Psychopharmacology (Berl) 1993;112:S40–54.

Menkes DB, Baraban JM, Aghajanian GK. Prazosin selectively antagonizes neuronal responses mediated by alpha1-adrenoceptors in brain. Naunyn Schmiedebergs Arch Pharmacol 1981;317:273–5.

Millan MJ, Gobert A, Lejeune F, Newman-Tancredi A, Rivet JM, Auclair A, et al. S33005, a novel ligand at both serotonin and norepinephrine transporters: I. Receptor binding, electrophysiological, and neurochemical profile in comparison with venlafaxine, reboxetine, citalopram, and clomipramine. J Pharmacol Exp Ther 2001;298:565–80.

Nasrallah HA. Atypical antipsychotic-induced metabolic side effects: insights from receptor-binding profiles. Mol Psychiatry 2008;13:27–35.

Nishitsuji K, To H, Shimizu T, Yanase Y, Yamada T, Hara C, et al. The pharmacokinetics and pharmacodynamics of tandospirone in rats exposed to conditioned fear stress. Eur Neuropsychopharmacol 2006;16:376–82.

Oehrberg S, Christiansen PE, Behnke K, Borup AL, Severin B, Soegaard J, et al. Paroxetine in the treatment of panic disorder. A randomised, double-blind, placebo-controlled study. Br J Psychiatry 1995;167:374–9.

Ohmori T, Abekawa T, Muraki A, Koyama T. Competitive and noncompetitive NMDA antagonists block sensitization to methamphetamine. Pharmacol Biochem Behav 1994;48:587–91.

Pudovkina OL, Cremers TIFH, Westerink BHC. Regulation of the release of serotonin in the dorsal raphe nucleus by α_1 and α_2 adrenoceptors. Synapse 2003;50:77–82.

Rea K, Folgering J, Westerink BHC, Cremers TIFH. α_1-Adrenoceptors modulate citalopram-induced serotonin release. Neuropharmacology 2010;58:962–71.

Richelson E, Souder T. Binding of antipsychotic drugs to human brain receptors focus on newer generation compounds. Life Sci 2000;68:29–39.

Rouquier L, Claustre Y, Benavides J. Alpha 1-adrenoceptor antagonists differentially control serotonin release in the hippocampus and striatum: a microdialysis study. Eur J Pharmacol 1994;261:59–64.

Santarelli L, Saxe M, Gross C, Surget A, Battaglia F, Dulawa S, et al. Requirement of hippocampal neurogenesis for the behavioral effects of antidepressants. Science 2003;301:805–9.

Selken J, Nichols DE. α_1-Adrenergic receptors mediate the locomotor response to systemic administration of (±)-3,4-methylenedioxymethamphetamine (MDMA) in rats. Pharmacol Biochem Behav 2007;86:622–30.

Stahl SM. Mechanism of action of serotonin selective reuptake inhibitors. Serotonin receptors and pathways mediate therapeutic effects and side effects. J Affect Disord 1998;51:215–35.

Vandermaelen CP, Aghajanian GK. Electrophysiological and pharmacological characterization of serotonergic dorsal raphe neurons recorded extracellularly and intracellularly in rat brain slices. Brain Res 1983;289:109–19.

Zhang W, Perry KW, Wong DT, Potts BD, Bao J, Tollefson GD, et al. Synergistic effects of olanzapine and other antipsychotic agents in combination with fluoxetine on norepinephrine and dopamine release in rat prefrontal cortex. Neuropsychopharmacology 2000;23:250–62.

Zohar J, Westenberg HG. Anxiety disorders: a review of tricyclic antidepressants and selective serotonin reuptake inhibitors. Acta Psychiatr Scand Suppl 2000;403:39–49.

Psychiatry Research: Neuroimaging ▮ (▮▮▮▮) ▮▮▮–▮▮▮

Contents lists available at SciVerse ScienceDirect

Psychiatry Research: Neuroimaging

journal homepage: www.elsevier.com/locate/psychresns

Impaired integrity of the brain parenchyma in non-geriatric patients with major depressive disorder revealed by diffusion tensor imaging

Khin K. Tha [a,*], Satoshi Terae [b,*], Shin Nakagawa [c], Takeshi Inoue [c], Nobuki Kitagawa [c], Yuki Kako [c], Yasuya Nakato [c], Kawser Akter Popy [b], Noriyuki Fujima [b], Yuri Zaitsu [b], Daisuke Yoshida [b], Yoichi M. Ito [d], Tamaki Miyamoto [e], Tsukasa Koyama [c], Hiroki Shirato [a]

[a] Hokkaido University Graduate School of Medicine, Department of Radiobiology and Medical Engineering, N-15, W-7, Kita-ku, Sapporo 060-8638, Japan
[b] Department of Diagnostic Radiology, Hokkaido University Graduate School of Medicine, N-15, W-7, Kita-ku, Sapporo 060-8638, Japan
[c] Department of Psychiatry, Hokkaido University Graduate School of Medicine, N-15, W-7, Kita-ku, Sapporo 060-8638, Japan
[d] Department of Biostatistics, Hokkaido University Graduate School of Medicine, N-15, W-7, Kita-ku, Sapporo 060-8638, Japan
[e] Department of Health Sciences, Hokkaido University Graduate School of Medicine, N-15, W-7, Kita-ku, Sapporo 060-8638, Japan

ARTICLE INFO

Article history:
Received 19 July 2011
Received in revised form
16 June 2012
Accepted 11 July 2012

Keywords:
Fractional anisotropy
Mean diffusivity
Voxel-based analysis
Histogram

ABSTRACT

Diffusion tensor imaging (DTI) is considered to be able to non-invasively quantify white matter integrity. This study aimed to use DTI to evaluate white matter integrity in non-geriatric patients with major depressive disorder (MDD) who were free of antidepressant medication. DTI was performed on 19 non-geriatric patients with MDD, free of antidepressant medication, and 19 age-matched healthy subjects. Voxel-based and histogram analyses were used to compare fractional anisotropy (FA) and mean diffusivity (MD) values between the two groups, using two-sample t tests. The abnormal DTI indices, if any, were tested for correlation with disease duration and severity, using Pearson product-moment correlation analysis. Voxel-based analysis showed clusters with FA decrease at the bilateral frontal white matter, anterior limbs of internal capsule, cerebellum, left putamen and right thalamus of the patients (uncorrected $P < 0.001$). Histogram analysis revealed lower peak position of FA histograms in the patients ($P = 0.00097$). FA values of the abnormal clusters and peak positions of FA histograms of the patients exhibited moderate correlation with disease duration and severity ($P < 0.05$). These results suggest implication of frontal-subcortical circuits and cerebellum in MDD, and the potential utility of FA in evaluation of brain parenchymal integrity.

1. Introduction

Major depressive disorder (MDD) is a common disorder with a chronic pattern of recurrence and a lifetime prevalence of 16.2% (Kessler et al., 2003). It is the fourth most disabling medical condition worldwide based on disability-adjusted life years (Greenberg et al., 1993). The neurobiology of MDD is not completely understood. A number of previous studies involving morphometric analysis using optical dissector methodology, voxel-based morphometry using magnetic resonance imaging (MRI), single photon emission computed tomography (SPECT), and positron emission tomography (PET) have reported a reduction in cortical thickness and the density of cortical neurons, as well as alterations in cerebral blood flow or glucose metabolism of cerebral cortices in MDD. These results are suggestive of gray matter pathology (Graff-Guerrero et al., 2004; Uranova et al., 2004; Egger et al., 2008; Fujimoto et al., 2008). On the other hand, recent converging evidence based on the findings of diffusion tensor imaging (DTI) is suggestive of abnormalities of white matter or frontal-subcortical circuits (e.g., Tekin and Cummings, 2002; Bae et al., 2006; Nobuhara et al., 2006; Shimony et al., 2009).

DTI is an MRI technique which can quantify white matter integrity noninvasively and in vivo (Moseley, 2002). This technique enables quantification of white matter integrity through its ability to detect motion of water molecules. Many studies suggest that DTI can uncover the microstructural white matter abnormalities that cannot be detected by other MRI techniques (e.g., Nagesh et al., 2008; Tha et al., 2010). It has also been reported that the abnormalities revealed by DTI correlate significantly with clinical severity in various white matter pathologies (e.g., Della Nave et al., 2007; Tha et al., 2010). Two major indices–fractional anisotropy (FA) and mean diffusivity (MD), are usually used to quantify microstructural white matter integrity by DTI (Moseley, 2002). FA quantifies the degree of directional coherence, whereas MD quantifies the degree of magnitude of water diffusion.

* Corresponding author. Tel.: +81 11 706 5977; fax: +81 11 706 7876.
E-mail addresses: kktha@med.hokudai.ac.jp (K.K. Tha), saterae@med.hokudai.ac.jp (S. Terae).

0925-4927/$ - see front matter © 2012 Elsevier Ireland Ltd. All rights reserved.
http://dx.doi.org/10.1016/j.pscychresns.2012.07.004

The major DTI indices are usually evaluated by either one or more of the following techniques: region-of-interest (ROI)-based analysis, tract (tractography)-based analysis, histogram analysis, and voxel-based analysis (Jones et al., 2005; Taoka et al., 2007). ROI-based and tract (tractography)-based analyses are usually chosen if there is known targeted anatomical area or tract to be evaluated. The latter two techniques are better suited if the area of involvement is not known, or when an a priori spatial selection and hypothesis are not made. In addition, the latter two techniques do not involve placement of ROI—which requires an operator with expertise in neuroanatomy and involves some inherent subjectivity (Marquez de la Plata et al., 2011). Previous DTI studies on MDD have been performed using ROI-based analysis, voxel-based analysis, and/ or tract (tractography)-based analysis (e.g., Taylor et al., 2004; Malykhin et al., 2008; Korgaonkar et al., 2011; Wu et al., 2011). Regarding selection of patients, the majority of these studies were performed on geriatric patients and the patients under antidepressant medication (e.g., Alexopoulos et al., 2002; Yang et al., 2007; Alexopoulos et al., 2008; Zou et al., 2008). The results of these studies revealed impaired white matter integrity in these patients. However, it is possible that the findings of these studies were confounded by age-related pathology and/or the effect of antidepressant medication (Korgaonkar et al., 2011). With aging, the FA values of all white matter tracts decrease and their MD values increase (Sala et al., 2012). There have also been a few reports about the effect of antidepressant medication on white matter integrity (Yoo et al., 2007; Sijens et al., 2008; Taylor et al., 2011). Normalization of FA and MD values of cerebral white matter after treatment with antidepressants such as citalopram, fluoxetine, and sertraline, as well as decrease in the FA values of the right posterior thalamic radiation following treatment with citalopram, have been documented—suggestive of the modification of white matter integrity by antidepressant medication. The number of DTI studies performed on non-geriatric patients who were free of antidepressant medication is limited (Li et al., 2007; Ma et al., 2007; Korgaonkar et al., 2011; Ouyang et al., 2011; Wu et al., 2011; Zhu et al., 2011). Although the results of these preliminary studies suggest impaired white matter integrity in MDD, the location of abnormalities is inconsistent among the studies and their results are not replicable (Korgaonkar et al., 2011; Wu et al., 2011)—calling for the need for further investigations.

This study was aimed to evaluate white matter integrity in non-geriatric (e.g., <65 years) patients with MDD who were free of antidepressant medication for at least 6 months, by using voxel-based and histogram analyses of DTI. It was hypothesized that these patients would have impaired integrity of white matter that could be depicted by DTI.

2. Methods

2.1. Participants

This prospective study was approved by the local institutional review board. Written informed consent was obtained from all participants.

The patients were recruited during a 35-month period (August, 2007 to March, 2010), at the Department of Psychiatry, Hokkaido University Hospital. Inclusion criteria for the patients were age between 20 and 64 years (Waxman et al., 1982; Korgaonkar et al., 2011), diagnosis of MDD according to the Diagnostic and Statistical Manual, Fourth Edition, Text Revision (DSM-IV-TR), and being free of antidepressant medication for at least 6 months. Exclusion criteria were absolute contraindications for MRI, comorbid axis I or II disorders, history of electroconvulsive therapy, history of diseases that might affect white matter integrity (e.g., infarct, hemorrhage, migraine), and significant abnormality on conventional MRI sequences {i.e., T2-weighted imaging (T2WI) and fluid-attenuated inversion recovery (FLAIR) imaging sequences}. Of 25 patients who fit the inclusion criteria, 19 patients were eligible for the study. No patients had any psychotic features. Eleven patients were never treated with antidepressants. The remaining eight patients had a previous history of medication with one or more antidepressant agents, but had been free of the medication for at least 6 months.

To obtain normal control data, MRI was also performed on 19 age-matched normal subjects. Exclusion criteria were absolute contraindications for MRI, axis I or II disorders, history of diseases that might affect white matter integrity, and any obvious abnormality on the conventional MRI sequences. Psychiatric diseases were excluded through a short-structured diagnostic interview (Mini-International Neuropsychiatric Interview; MINI)(Sheehan et al., 1998).

The demographic characteristics of the patients and control subjects are summarized in Table 1.

2.2. MRI

In all patients, MRI was performed on the day of first clinical consultation for the current episode or the day on which the diagnosis was made. There was no undue delay in the prescription of antidepressant medication for the purpose of this study.

MRI was performed using a 1.5 T imager and a standard head coil. The participants were asked not to move their heads during the examination, and foam pads were used to minimize involuntary head motion. An axial single-shot spin-echo echo-planar imaging sequence was used for DTI. Parameters included the following: repetition time (TR)/echo time (TE), 5100/139 ms; b value (b), 1000 s mm^{-2}; diffusion-encoding gradients, 12 directions; number of signals acquired, two; field of view (FOV), 240 × 240 mm; matrix size, 128 × 128 (interpolated into 256 × 256); pixel size, 1.875 × 1.875 mm; intersection gap, 1.5 mm; section thickness, 5 mm; and section number, 23. Echo-planar images with no diffusion weighting (b=0 s mm^{-2}) were also obtained for use in spatial normalization and coregistration.

In addition to DTI, axial fast spin-echo T2WI (TR/TE, 4540/96 ms; effective echo train length (ETL_{eff}), 7; FOV, 180 × 240 mm; matrix size, 185 × 448; pixel size, 0.973 × 0.536; intersection gap, 1.5 mm; section thickness, 5 mm; and section number, 23), axial fast FLAIR imaging (TR/TE, 9000/104 ms; inversion time (TI), 2500 ms; FOV, 180 × 240 mm; matrix size, 192 × 256; pixel size, 0.938 × 0.938; intersection gap, 1.5 mm; section thickness, 5 mm; and section number, 23), and three-dimensional T1-weighted imaging with a magnetization-prepared rapid acquisition gradient-echo (MPRAGE) sequence (TR/TE, 1900/3.9 ms; TI, 1100 ms; flip angle, 15°; FOV, 250 × 250 mm; matrix size, 256 × 256; pixel size, 0.978 × 0.978; gapless; section thickness, 1 mm; imaging plane, coronal; and section number, 240) were also acquired.

Table 1
The demographic characteristics of the patients and normal subjects.

	Patients (n=19)	Control subjects (n=19)	P-value
Age	38.6 ± 13.5 years (20–61)[a]	36.5 ± 12.5 years (22–60)[a]	0.613[b]
Gender (men/women)	12/7	13/6	0.729[c]
Previous history of antidepressant medication (present/absent)	8/11	–	–
Previous episodes (present/absent)	5/14	–	–
Total disease duration	18.37 ± 28.17 months (1–96)[a]	–	–
Duration of current episode	5.89 ± 5.69 months (1–24)[a]	–	–
HDRS-17	19.00 ± 4.00 (11–26)[a]	–	–
GAF	43.79 ± 9.90 (28–58)[a]	–	–
MADRS	26.21 ± 5.57 (20–39)[a]	–	–
CGI-S	4.68 ± 0.89 (3–6)	–	–

[a] Data are presented in mean ± standard deviation (range).
[b] The statistical significance was evaluated by using two-sample t test.
[c] Or χ^2 test.

Please cite this article as: Tha, K.K., et al., Impaired integrity of the brain parenchyma in non-geriatric patients with major depressive disorder revealed by.... Psychiatry Research: Neuroimaging (2012), http://dx.doi.org/10.1016/j.pscychresns.2012.07.004

2.3. Image processing and analysis

2.3.1. Construction of FA and MD maps

FA and MD maps were constructed on a workstation from the diffusion tensor images, according to the methods of Basser and Pierpaoli (1996) (Dr. View/LINUX R2.5.0; AJS, Tokyo, Japan). To ensure computation only of tensors inside the brain rather than the surrounding air, a brain mask, computed based on the signal intensity of diffusion tensor images, was applied to the diffusion tensor images.

2.3.2. Voxel-based analysis

The steps involved all closely followed those of a previous report (Tha et al., 2010). First, the customized FA and MD templates were built from the FA and MD maps of the control subjects. For this purpose, the echo-planar images with no diffusion weighting of each control subject were first warped to the standard echo-planar template of statistical parametric mapping software (SPM5, www.fil.ion.ucl.ac.uk), by using default parameters. This transformation information was then applied to the FA and MD maps of each subject. The warped FA and MD maps were averaged and smoothed with a 6-mm full-width half-maximum (FWHM) Gaussian kernel, to form the customized FA and MD templates. Visual review of the output images was performed to ensure that no obvious registration error was encountered.

Next, the native FA and MD maps of all patients and control subjects were warped to the customized FA and MD templates, respectively. The parameters applied were the same as those described previously. Visual review of all warped images was performed to ensure that no obvious registration error was encountered. Individual maps were then smoothed with a 6-mm FWHM Gaussian kernel.

Warped and smoothed FA and MD maps of the patients and control subjects were next compared voxel-by-voxel by using a two-sample t test. The analysis was restricted to the area covered by a mask (void of cortical gray matter and ventricles)—which was developed from the customized FA template by discarding voxels with an FA value of less than 0.2 (MRIcron, www.cabiatl.com/mricro/mricron). Uncorrected P value of less than 0.001 and a cluster size of greater than 50 voxels were considered significant. The FA and MD values of the clusters in the patients which differed significantly from the control subjects, if any, were measured (MarsBaR, www.marsbar.sourceforge.net).

2.3.3. Histogram analysis

The steps involved were the same as those of a previous report (Mori et al., 2008), except that white matter masks were used in this study instead of whole-brain binary masks. In brief, the axial sections of individual MPRAGE images of each participant were coregistered to the echo-planar images with no diffusion weighting (SPM5). Visual review of the output images was performed to ensure that no obvious registration error was encountered. From the axial sections of the MPRAGE images, white matter was automatically segmented by using the default parameters of SPM5. Each segmented image was checked to ensure accuracy. The segmented white matter (the segmented area also included the thalami and part of basal ganglia.) was used to serve as individual white matter masks. Each white matter mask was applied to the FA and MD maps of the corresponding participant (MRIcron). Histograms were then calculated for the masked FA and MD maps of each participant (ImageJ, www.rsb.info.nih.gov/ij). The bin width of the FA histograms was set as 0.01(between 0.0 and 1.0), and that of MD histograms was set as 5×10^{-5} (between 0.0 and 0.0055). To correct skewness, the natural logarithmic transformation of FA and MD bins was used. To correct for individual differences in the brain volume, each histogram was normalized by the total number of voxels contributing to the histogram. From each histogram, the peak height and location were extracted. These histogram parameters were then compared between the two groups, by using two-sample t test. A P value of less than 0.05 was set to determine statistical significance.

2.3.4. Correlation between the altered DTI indices and clinical variables

The absolute values of altered DTI indices of the patients (for voxel-based analysis, FA or MD values of the clusters which differed significantly from the control subjects; for histogram analysis, the peak height or position of FA or MD histograms which differed significantly from the control subjects), if any, were tested for correlation with total disease duration, duration of current disease episode, the scores that assess clinical severity {17-item Hamilton depression rating scale (HDRS-17) (Williams, 1988), global assessment of functioning (GAF)(-Hall, 1995), Montgomery-Åsberg depression rating scale (MADRS) (Montgomery and Åsberg, 1979), clinical global impression-severity (CGIS)(Guy, 1976)}, and age, by using Pearson product-moment correlation analysis. The difference in the absolute values of altered DTI indices between the gender groups was evaluated by using two-sample t test. For all conditions, a P value of less than 0.05 was considered to indicate a significant difference. Correction for multiple comparisons was not performed.

3. Results

3.1. Voxel-based analysis

The results of voxel-by-voxel comparison of FA values between the two groups are shown in Fig. 1. Clusters with a significant decrease in FA values were observed at the bilateral frontal white matter, anterior limbs of the internal capsule, the left putamen, the mediodorsal nucleus of the right thalamus, and the anterior and superior aspect of bilateral cerebellar hemispheres of the patients. These clusters persisted even after controlling for age and gender. There were no significant clusters with an increase in the FA or altered MD values in the patients.

3.2. Histogram analysis

The mean FA and MD histograms of the patients and control subjects are shown in Fig. 2 and Fig. 3, respectively. The peak position of the FA histograms of the patients was significantly lower than that of the control subjects ($P=0.00097$). The results revealed a tendency toward a higher peak height in the MD

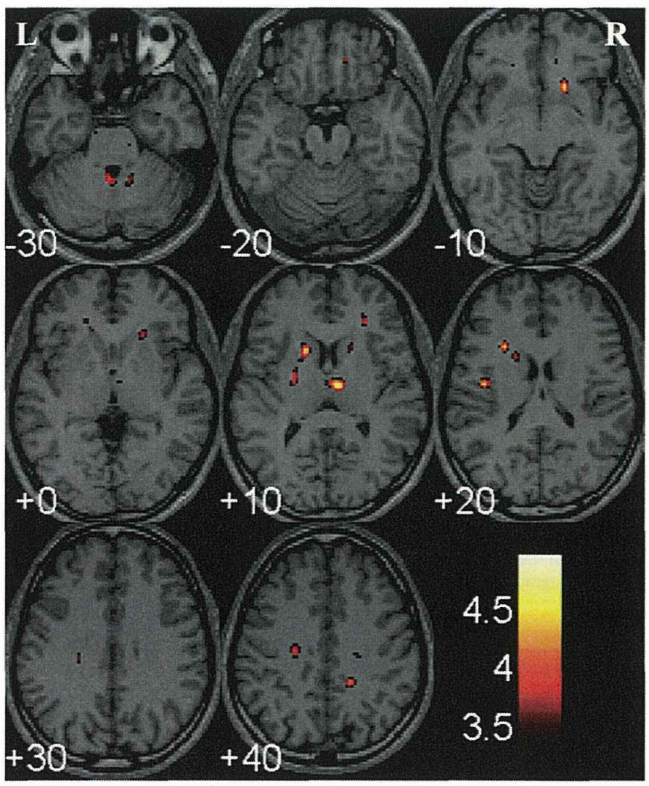

Fig. 1. The results of voxel-by-voxel comparison of FA values between the patients and control subjects, superimposed on a T1-weighted template. Clusters with significant decrease in FA values (uncorrected $P<0.001$, minimum cluster size=50 voxels) are observed in the patients, in the right frontal white matter {(i) MNI coordinates: $x=12$, $y=43$, $z=-18$, cluster size=70 voxels, $t=4.34$; (ii) MNI coordinates: $x=37$, $y=-19$, $z=59$, cluster size=100 voxels, $t=4.43$}, left frontal white matter (MNI coordinates: $x=-24$, $y=-21$, $z=34$, cluster size=135 voxels, $t=4.53$), right anterior limb of internal capsule (MNI coordinates: $x=17$, $y=18$, $z=-9$, cluster size=111 voxels, $t=4.63$), left anterior limb of internal capsule (MNI coordinates: $x=-14$, $y=14$, $z=9$, cluster size=135 voxels, $t=4.62$), left putamen (MNI coordinates: $x=-24$, $y=-7$, $z=7$, cluster size=74 voxels, $t=4.12$), the mediodorsal nucleus of right thalamus (MNI coordinates: $x=7$, $y=-14$, $z=8$, cluster size=138 voxels, $t=4.98$), right cerebellar hemisphere (MNI coordinates: $x=22$, $y=-48$, $z=-27$, cluster size=83 voxels, $t=4.14$), and left cerebellar hemisphere (MNI coordinates: $x=-3$, $y=-49$, $z=-25$, cluster size=50 voxels, $t=4.17$). Look-up table represents the t values. L and R represent the left and right sides, respectively.

Please cite this article as: Tha, K.K., et al., Impaired integrity of the brain parenchyma in non-geriatric patients with major depressive disorder revealed by.... Psychiatry Research: Neuroimaging (2012), http://dx.doi.org/10.1016/j.pscychresns.2012.07.004

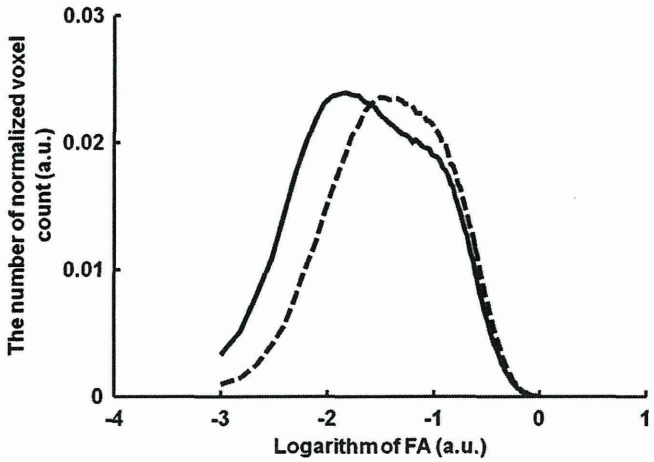

Fig. 2. The mean FA histograms of the patients (solid line) and control subjects (dotted line). The average number of normalized voxels is plotted against the logarithm of the FA values. The peak position of FA histogram of the patients is significantly lower than that of normal subjects ($P=0.00097$). The peak height of FA histograms does not vary significantly.

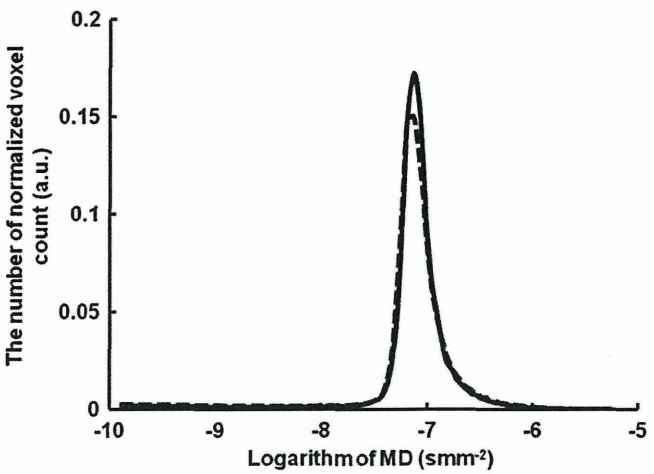

Fig. 3. The mean MD histograms of the patients (solid line) and control subjects (dotted line). The average number of normalized voxels is plotted against the logarithm of the MD values. No significant difference in the peak position or height of MD histograms is observed.

histograms of the patients, but this alteration was not statistically significant ($P=0.11615$). The peak height of the FA histograms and the peak position of the MD histograms did not vary significantly between the two groups ($P=0.79527$ and $P=1$, respectively).

3.3. Correlation between the altered DTI indices and clinical variables

The results of the tests of correlation between the altered DTI indices of the patients and clinical variables are summarized in Table 2 and Fig. 4. Of clusters with a significant FA decrease, the FA value of the right frontal white matter ($x=12$, $y=43$, $z=-18$) revealed moderate negative correlation with duration of current disease episode. The right frontal white matter ($x=37$, $y=-19$, $z=59$) and the right anterior limb of internal capsule revealed moderate negative correlation with the GAF. The left anterior limb of the internal capsule exhibited a moderate positive correlation with total disease duration. The right cerebellar hemisphere exhibited a moderate positive correlation with the HDRS-17. The peak position of the FA histogram had a moderate positive correlation with total disease duration and the duration of the current disease episode. The FA value of the left cerebellar hemisphere revealed a moderate positive correlation with age. There was no significant difference in the regional FA values or the peak positions of FA histograms, between the gender groups ($P>0.220$).

4. Discussion

This study evaluated white matter integrity in non-geriatric patients with MDD by using DTI. Two semiautomated/automated methods—voxel-based and histogram analyses, were used for the analysis. Both methods were able to identify abnormalities in the patients. Voxel-based analysis showed clusters with a significant decrease in FA at the bilateral frontal white matter and the anterior limbs of internal capsule. In addition to cerebral white matter, clusters with a significant decrease in the FA were also observed in the subcortical gray matter (including the left putamen and the mediodorsal nucleus of the right thalamus) and bilateral cerebellar hemispheres. In histogram analysis, a lower peak position (i.e., "shift toward the left") of the FA histograms of the patients was observed, indicative of inclusion in the patients with a greater number of voxels with low FA values compared to normal subjects.

Decrease in the FA is reflective of an impaired directional coherence of the brain microstructures (Moseley, 2002). The histological correlates of decrease in the FA, as revealed by the reports of autopsies and biopsies of various diseases of the brain and experimental models, include larger axonal spacing, a decrease in axon count, diameter and density, and myelin loss (Beaulieu, 2011). The autopsy reports of patients with MDD are scarce. Limited evidence has suggested myelin pallor in the white matter underlying prefrontal cortex (Regenold et al., 2007). Taken together with the knowledge that myelin pallor results from demyelination, incomplete myelination of axons, axonal loss, or axonal agenesis, our finding of FA decrease in the bilateral frontal white matter and anterior limbs of internal capsule may reflect axon and/or myelin abnormality. Histological proof regarding the changes of the putamen, thalamus, and cerebellar hemispheres in MDD is lacking. The exact pathological process that occurs in these structures is thus not known. Nonetheless, from the findings of neuronal loss in some subcortical structures such as the nucleus basalis, substantia nigra, and raphe nucleus (Tsopelas et al., 2011), it is possible that similar pathological changes are encountered. Axon and/or myelin abnormality are also possible, as axon and myelin are the components of these structures.

Human behaviors (executive functions, social behavior, and motivational states) are mediated mainly by three parallel frontal-subcortical circuits (Tekin and Cummings, 2002). These circuits originate from the dorsolateral prefrontal region, lateral orbitofrontal region, and anterior cingulate portion of the frontal cortex; and form connections to the striatum, basal ganglia, and thalamus. From the thalamus, fibers of these circuits loop back to the cortex of origin. In addition to forming closed loops, these circuits form open connections with the other areas of the frontal lobe, parietal and temporal lobes, amygdala, hippocampus, substantia nigra, subthalamic nucleus, hypothalamus, and the brainstem. Our findings of decrease in the FA at the bilateral frontal white matter, anterior limbs of internal capsule, left putamen and right thalamus are suggestive of impaired integrity or dysfunctioning of these circuits. Although mediation of human behavior by these circuits is well-established, emerging evidence is suggestive of participation of the cerebellum in the regulation of mood and cognition as well (Diamond, 2000). The cerebellum forms anatomical and functional connections with the prefrontal

Please cite this article as: Tha, K.K., et al., Impaired integrity of the brain parenchyma in non-geriatric patients with major depressive disorder revealed by.... Psychiatry Research: Neuroimaging (2012), http://dx.doi.org/10.1016/j.pscychresns.2012.07.004